

## THE COMPOSITIONAL EVOLUTION OF APATITE IN THE WEATHERING PROFILE OF THE CATALÃO I ALKALINE-CARBONATITIC COMPLEX, GOIAS, BRAZIL

M. CRISTINA M. DE TOLEDO<sup>§</sup>

*Instituto de Geociências, Universidade de São Paulo, Rua do Lago, 562 – 05508-080 São Paulo, SP, Brasil*

SARA L.R. LENHARO<sup>§</sup>

*Universidade Estadual do Norte Fluminense Darcy Ribeiro, Av. Alberto Lamego, 2000 – Campos dos Goytacazes – 28013-600 Rio de Janeiro, RJ, Brasil*

VIVIANE C. FERRARI

*Instituto de Geociências, Universidade de São Paulo, Rua do Lago, 562 – 05508-080 São Paulo, SP, Brasil*

FRANÇOIS FONTAN<sup>§</sup> AND PHILIPPE DE PARSEVAL<sup>§</sup>

*CMTG–CNRS 5563, Laboratoire de Minéralogie, Université Paul Sabatier, Observatoire Midi-Pyrénées, 14, Av. Edouard Belin, F-31400 Toulouse, France*

GÉRARD LEROY<sup>§</sup>

*Faculté d'Odontologie, Place de Verdun, F-59000 Lille, France*

### ABSTRACT

The mineralogical, micromorphological, geochemical and crystallographic characteristics of the different types of apatite from the Catalão I alkaline-carbonatitic complex, Goiás, Brazil, were determined by optical and scanning-electron microscopy, electron-microprobe analysis, Raman micro-spectroscopy, X-ray diffraction, thermodifferential and thermogravimetric analyses and Fourier-transform infrared spectroscopy. There are three main generations of apatite: igneous, postmagmatic or hydrothermal, and supergene. The composition of apatite of each generation has been determined. Data from primary apatite affected by weathering processes show compositional changes prior to the total destruction of grains. The main geochemical trends observed from the first to the third generation are: a) increase in  $\text{CO}_3^{2-}$  (that replaces  $\text{PO}_4^{3-}$ ), in F (which follows the incorporation of carbonate), in Ca (owing to loss of substituting cations, mainly Sr, Na, and REE) and in the ratio  $\text{CaO/P}_2\text{O}_5$  (increase of Ca due to loss of the cations that substituted for Ca, and decrease of  $\text{PO}_4^{3-}$ , partially replaced by  $\text{CO}_3^{2-}$ ), b) decrease in Si and P (replaced by C), in Sr, Na and REE (replaced by Ca) and in analytical totals (owing to an increase in components not detected using the electron microprobe, such as C and OH). These chemical changes, along with contemporaneous modification of the morphology of the apatite grains, contribute to an undesirable behavior of the apatite ore, once submitted to processes of industrial concentration. The types of apatite and the processes of their formation here defined and established for the Catalão I alkaline-carbonatitic complex are quite common and widely distributed in all carbonatitic phosphatic raw materials in Brazil, as observed in previous studies. The coexistence of these morphological and compositional varieties is responsible for the heterogeneity and complexity of these ores.

*Keywords:* apatite, phosphate, phosphate ore, carbonatite, weathering, lateritization, hydrothermal alteration, geochemistry, micromorphology, applied mineralogy, Catalão I carbonatite, Goiás, Brazil.

### SOMMAIRE

Nous avons déterminé les caractéristiques minéralogiques, micromorphologiques, géochimiques et cristallographiques des différents types d'apatite provenant du massif alcalin-carbonatitique de Catalão I, à Goiás, Brésil, en appliquant les techniques suivantes: microscopie optique et électronique à balayage, analyses à la microsonde électronique, microspectroscopie de Raman,

<sup>§</sup> *E-mail addresses:* mcristol@usp.br, sara@lenep.uenf.br, viviane\_ferrari@uol.com.br, fontan@lmtg.obs-mip.fr, parseval@insa.fr, gleroy@univ-lille2.fr

diffraction X, analyses thermodifférentielle et thermogravimétrique, et spectroscopie infrarouge avec transformation de Fourier. Nous distinguons trois générations principales d'apatite: ignée, postmagmatique ou hydrothermale, et supergène. Nous avons déterminé la composition de l'apatite de chaque génération. Les données sur l'apatite primaire affectée par processus de lessivage révèlent la présence de changements dans la composition précédant la destruction totale des grains. Parmi les transformations principales, allant de la première à la troisième génération, on voit: a) une augmentation de la proportion de  $\text{CO}_3^{2-}$  (qui remplace le  $\text{PO}_4^{3-}$ ), de F (qui accompagne le carbonate), de Ca (à cause de la perte des cations qui le remplacent, surtout Sr, Na, et les terres rares) et du rapport  $\text{CaO/P}_2\text{O}_5$  (augmentation du Ca à cause de la perte des autres cations qui prennent la place du Ca, et diminution de la proportion de  $\text{PO}_4^{3-}$ , partiellement remplacée par le  $\text{CO}_3^{2-}$ ), et b) une diminution de la proportion du Si et du P (remplacés par le C), du Sr, Na et des terres rares (remplacés par le Ca) et des totaux analytiques (à cause de l'augmentation de la proportion des composants non décelables avec une microsonde électronique, par exemple C et OH). Ces changements chimiques, accompagnés de modifications morphologiques des grains d'apatite, contribuent à un comportement indésirable du minerai d'apatite, une fois dans le circuit de concentration industrielle. Les types d'apatite et les processus de leur formation, tels que définis ici, et établis pour le cas du complexe de alcalin-carbonatitique de Catalão I, sont communs et répandus dans tous les gisements carbonatitiques de matériaux phosphatés au Brésil, comme le révèlent les travaux antérieurs. La coexistence de ces variantes morphologiques et compositionnelles serait responsable de l'hétérogénéité et la complexité de ces minerais.

(Traduit par la Rédaction)

*Mots-clés:* apatite, phosphate, minerai phosphaté, carbonatite, lessivage, latéritisation, altération hydrothermale, géochimie, micromorphologie, minéralogie appliquée, carbonatite de Catalão I, Goiás, Brésil.

## INTRODUCTION

Apatite-group minerals [ $\text{Ca}_5(\text{PO}_4)_3(\text{F}, \text{OH}, \text{Cl})$ ] constitute an important mineral resource. Apatite accumulations are associated with alkaline-carbonatitic complexes, with several examples in Brazil. Accumulations of apatite are mainly associated with lateritic processes (Rodrigues & Lima 1984), and also may result from sedimentary (marine phosphorites) and organic processes (guano). Apatite is known to be resistant to weathering in the first stages of weathering of carbonatitic rocks (Altschuller 1973, Flicoteaux & Lucas 1984), and may form lateritic ore deposits, which are very important in Brazil. However, in tropical environments, acid conditions arise after the complete weathering of carbonates, and lead to the weathering of apatite. Phosphorus is released from apatite to form new mineral phases, and to participate in supergene biogeochemical processes. The changes in primary apatite during the weathering and the newly formed phases may diminish the quality of the ore, because morphological and physicochemical characteristics do not allow industrial recovery (Toledo *et al.* 1999).

The Brazilian lateritic phosphatic ores, exploited by mining companies such as Fosfértil, Bunge, and Socal, contain several morphological types of apatite, formed during the entire evolution of the igneous complexes, starting from igneous apatite inherited from fresh rock. Our aim in this paper is to describe the textural, structural, and chemical attributes of the various types of apatite at the Catalão I alkaline-carbonatite complex. We emphasize those properties that determine how well or how poorly the apatite can be industrially recovered. The study was carried out using mineralogical, micromorphological, geochemical and crystallographic data, and observations on samples of both fresh igneous rocks and the products of their weathering.

## BACKGROUND INFORMATION

### *Apatite*

A voluminous bibliography has shown that starting from pure fluorapatite,  $\text{Ca}_{10}(\text{PO}_4)_6\text{F}_2$ , a great variety of substitutions at all crystallochemical sites may occur, leading to differences in solubility and physical and physicochemical behavior, which are extremely important for all branches related to apatite uses and studies (Kohn *et al.* 2002).

The majority of the bibliographic references mentioned here use the double formula for the apatite [ $\text{A}_{10}\text{X}_6\text{Y}_2$ ], and the same will be done here, to simplify comparisons. Various ways of calculating a structural formula for apatite have been presented in the literature: a) on the basis of the total number of oxygen atoms or anionic content (Roeder *et al.* 1987, Treloar & Colley 1996, Rønsbo 1989, Rae *et al.* 1996), b) on the basis of cationic sum at the A position plus the cation sum at the X or phosphorus position (Fleet & Pan 1995, Prins 1973), c) on the basis of the sum of ions at the X position (Fransolet & Schreyer 1981), and d) on the basis of number of cations in position A (Le Bas & Handley 1979, Sommerauer & Katz-Lehnert 1985, Liu & Comodi 1993).

It is quite rare to find a 10:6 (= 1.667) ratio between the occupancy of the A site (cations) and X site (P position), which corresponds to the ideal stoichiometric occupancy. In general, observed values of A:X are greater than 1.667, indicating a deficit in the X site or a cation excess, which could be accommodated in cavities in the structure (or both).

In the data of Roeder *et al.* (1987), for instance, among fourteen compositions reported from different localities, ten of them present deficits in the X position. In another example, all average compositions of apatite

from alkaline-carbonatitic complexes presented by Le Bas & Handley (1979) display the same deficit.

In addition, some constituents of apatite are difficult to treat analytically, and their concentrations are commonly calculated by difference. Some investigators, such as Le Bas & Handley (1979) and Sommerauer & Katz-Lehnert (1985), who also dealt with alkaline-carbonatitic complexes, added  $\text{CO}_3^{2-}$  to complete the *X* site without any verification of its presence in the apatite being studied. In the same way,  $\text{OH}^-$  is used to adjust the structure to the expression  $2 - \text{F}^- = \text{OH}^-$ , without testing for its presence by infrared or Raman spectroscopy, and without considering the possibility that part of the  $\text{F}^-$  may be located outside the channel (Regnier *et al.* 1994). In this case,  $\text{OH}^-$  calculation on the basis of electrical charge seems to be the better technique.

As summarized by Toledo & Pereira (2001), there are several uncertainties in determining the amount of  $\text{CO}_3^{2-}$  and  $\text{OH}^-$ , which are commonly incorporated in the structure and must be considered in a calculation of the structural formula. Another point is the position of  $\text{CO}_3^{2-}$ ; normally, it is admitted that the carbonate anion of natural apatite is at the *X* position (substituting for the phosphate anion, defining type-*B* apatite), but recently some investigators have found  $\text{CO}_3^{2-}$  in the channels (Comodi & Liu 2000), substituting for the monovalent anions at the *Y* position (type-*A* apatite).

In relation to  $\text{F}^-$ , there seems to be a consensus in the majority of the crystallographic studies that this anion may also be present outside the structural channels, following the  $\text{CO}_3^{2-}$  that substitutes for  $\text{PO}_4^{3-}$ , and promoting charge equilibrium. This balance may be done either in the proportion 1  $\text{F}^-$  for each  $\text{CO}_3^{2-}$ , as suggested in the majority of papers (Regnier *et al.* 1994, among others), or in the maximum proportion of 0.4  $\text{F}^-$  for each 1  $\text{CO}_3^{2-}$ , as indicated by McClellan (1980). The charge balance due to substitution of carbonate for phosphate anions may also be done by either  $\text{OH}^-$  entrance or creation of vacancies in the cationic position (Vignoles & Bonel 1978). The  $\text{F}^-$  ion and  $\text{OH}^-$  group cause a departure from the stoichiometric formula but perform a fundamental function in the electrical charge of the structure.

The diversity of aspects to be considered in the establishment of a method for the calculation of a structural formula suggests that each method will be subject to criticism. However, our attempt at determining one of the constituents that is difficult to document ( $\text{CO}_3^{2-}$ ), applying different approaches, is a contribution to more realistic calculations.

#### *Newly formed phosphates*

Aluminum plays an important role in the genesis of phosphates in superficial environments (Vieillard *et al.* 1979, Toledo *et al.* 1997, 2002). Aluminum deficiency in the weathering mantle, which is the case of the complexes where the carbonatite displays lateral and verti-

cal continuity, determines the precipitation of supergene apatite, chemically different from the primary one but preserving a high grade of apatite-bound phosphate in the whole material. On the other hand, in weathering profiles derived from zones of the alkaline-silicate rocks in the same complexes, aluminum is present and leads to extensive formation of aluminum phosphate. This formation of supergene apatite where Al is not available, and of aluminum phosphate where Al is present, is observed in several Brazilian carbonatite complexes, including Juquiá (Alcover Neto & Toledo 1993), Tapira (Ferrari *et al.* 2001), and Catalão I (Toledo 2000); all are sites of important phosphate mines in Brazil.

At Catalão I, previous studies (Toledo 2000) have shown both situations: apatite and aluminum phosphates are found in the weathering mantle owing to the heterogeneity of original rocks, composed of a mixed body of aluminum silicate and carbonatitic rocks.

#### GEOLOGICAL SETTING

The Catalão I Complex belongs to the Alto Paranaíba alkaline-carbonatitic province, along with several other complexes (Fig. 1a). These bodies were emplaced along deep northwest-trending faults related to the Alto Paranaíba cratonic arc, between the Paraná Basin and the São Francisco craton. An Upper Cretaceous age ( $85.0 \pm 0.9$  Ma) was obtained for syenites by Amaral *et al.* (1967), as recalculated by Sonoki & Garda (1988). Eby & Mariano (1986) determined an age of 114 Ma using fission-track analysis in apatite.

The Catalão I Complex has a high relief and is surrounded by a ring of quartzite; mica schists of the Mesoproterozoic Araxá Group are found outside this ring (Fig. 1b). A weathering mantle more than 100 m thick was developed over the intrusive body, and contains abundant residual apatite, pyrochlore, monazite, Ti-bearing minerals (perovskite, ilmenite, and anatase), and vermiculite. The intrusion consists of dunite, pyroxenite, phoscorite, phlogopitite, carbonatite and volcanoclastic rocks. From drill holes, outcrops and open pits, Ribeiro (1998) made a geological map of the Fوسفertil Co. area (Fig. 1b), and showed an association of carbonatite and phlogopitite, zones of carbonatite enriched in either Nb and Ba or Mg and the rare-earth elements (REE), and zones of hydrothermally altered volcanoclastic rocks with monazite mineralization. The geological, geochemical, petrological and mineralogical features of the Complex have been studied by Carvalho (1974), Araújo & Gaspar (1992), Lenharo (1994), Lápido-Loureiro (1995), Pereira (1995), Oliveira & Imbernon (1998), Toledo (1999, 2000), and Toledo *et al.* (1998, 1999, 2002). Of the main concentrations of apatite, pyrochlore, monazite, anatase and vermiculite already characterized in the Complex, only the first two are being exploited; apatite-bound phosphate is mined by the Fوسفertil and Copebrás companies, and niobium is exploited by Mineração Catalão Co.

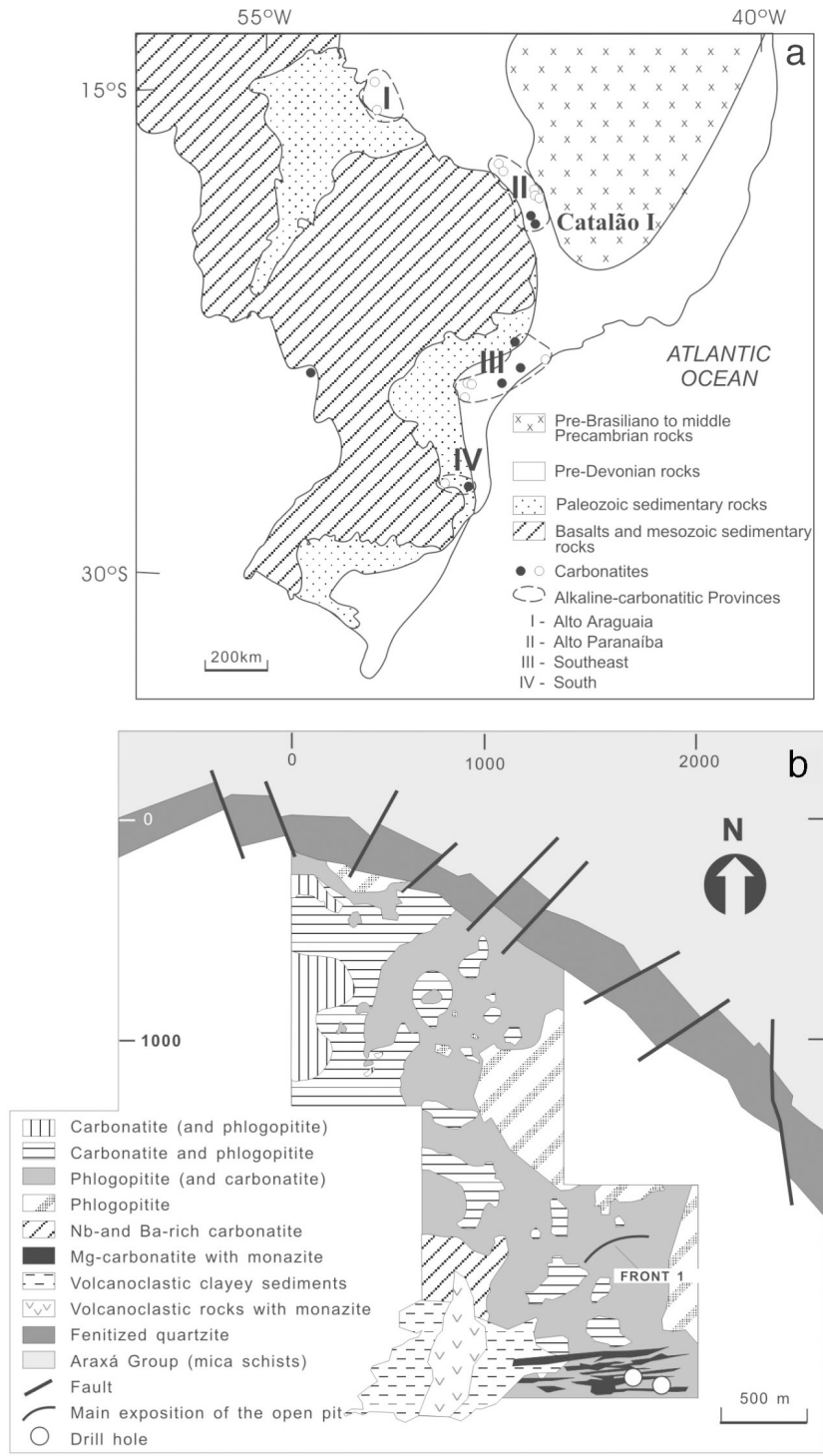


FIG. 1. Geological map of southeastern Brazil displaying the alkaline-carbonatitic complexes (Rodrigues & Lima 1984) (a), and geological map of the Catalão I complex (Ribeiro 1998) (b), with the location of the open pit (front 1) and the drill holes sampled.

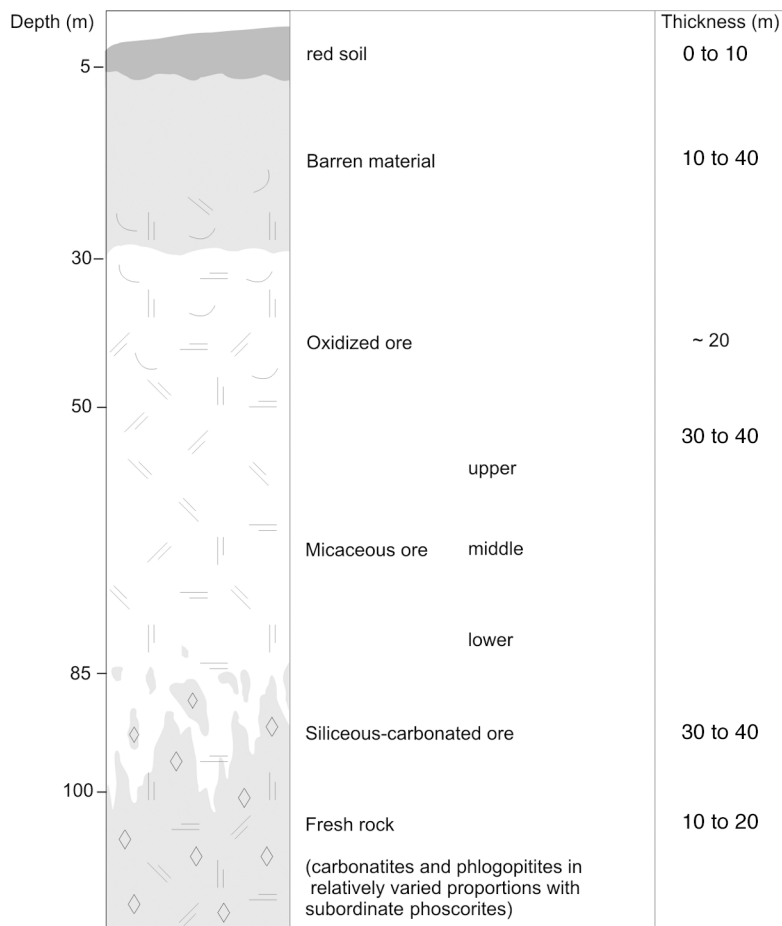


FIG. 2. Schematic weathering profile at the Catalão I phosphate mine, based on qualitative parameters of weathering, such as state of disintegration of the rock, color, the proportion of micaceous and clay minerals. The thickness and depth indications follow data from Ribeiro (1998), and material names are the same as used by the mining company. Weathering features can be found even deeper than 100 m, as indicated in Figure 3h.

SAMPLES AND ANALYTICAL METHODS

This study was based on more than 150 samples of both fresh igneous rocks and products of their weathering, sampled from the main open pit, named "Front 1" (80 weathered samples, from the surface to a depth of 80 m), some isolated samples from other exposures of weathering profiles on roads crossing the area, and from two drill holes (F58-03: 29 samples, from a depth of 253 m to the surface, with fresh rock beyond 110 m, and weathered rock from there toward the surface, and F56-07: 43 samples, from a depth of 327 m to the surface, with fresh rock beyond 150 m, and weathered rock

from there to the surface). These samples were collected for this research with the support of Brazilian official institutions and the Fosfértil Mining Co. Drill holes and Front 1 are located in Figure 1b.

A schematic profile showing the development of weathering on a phosphate-mineralized area (Fig. 2) was established on the basis of 1) the state of disintegration of the rock, 2) the relative amount of fresh and weathered material, 3) the color, and 4) the proportion of micaceous and clay minerals. The thickness and material names found in Figure 2 follow the conventions of Ribeiro (1998). In fact, the limits between different levels of weathering are very variable, and weathering fea-

tures can be found even deeper than 100 m. We use here the mine terminology: "fresh rock" refers to carbonatite and phlogopite in variable proportions, with subordinate phoscorite. There is also some silicified carbonatite. "Siliceous carbonated ore" refers to fresh blocks within friable material of dominant grey color representing the bottom of the weathering profile. "Micaceous ore" is subdivided into lower, middle and upper portions, mainly without preserved textures. The lower portion is yellow-orange in color, centimeters to tens of meters in thickness, with a large amount of phlogopite; the middle portion has a yellow-ochre color, with partially preserved phlogopite, and in the upper portion, materials with and without preserved primary textures alternate, composed of ochre or ochre-yellow and argillaceous material, with vermiculite. "Oxidized ore" is dark ochre in color, with occasional relict silicified carbonatitic veins. "Barren material" is yellow-ochre in color, and mainly without primary textures. Finally, "red soil" constitutes the pedogenetic horizons; it has not been studied and is commonly lacking owing to mining activities and sampling for mineralogical research.

Mineralogical identification was made by X-ray diffraction (XRD). Thin sections of all samples were studied with a polarizing microscope (OM). Selected natural fragments were studied by scanning electron microscopy (SEM) with energy-dispersion spectroscopy (EDS). The last two techniques allow us to recognize the morphological types of apatite grains and their mutual and spatial relationships, and to deduce genetic affinities among them. In addition, these observations allow us to define a qualitative index of morphological and textural characteristics based on the presence of discontinuities, their degree of filling, the shape and fabric of the grains. This study was also used to select areas for electron-microprobe (EMP) analysis of each morphological type. The terminology used for supergene textures is based on Brewer (1964) and Delvigne (1998).

In the geochemical and crystallographic studies, the various textural types and generations of apatite were analyzed by EMP for major, minor and trace elements. Raman micro-spectroscopy (RM) and Fourier-transform infrared spectroscopy (FTIR) were used to estimate the presence and crystallographic position of the  $\text{CO}_3^{2-}$  and to assess the presence of  $\text{OH}^-$ . We also used XRD data to calculate the unit-cell parameters of some samples considered to contain a single phase; these parameters may be used to infer chemical and crystallographic characteristics. We found the SEM, OM and EMP techniques applied to undisturbed samples to be very important in the study of the finely heterogeneous material. We used XRD on powder samples composed of more than one generation of apatite where there was no possibility of separating the phases. We applied FTIR to some samples considered to contain a single phase. We applied RM to samples of all types of apatite (see below), although calculations of  $\text{CO}_2$  content were only possible for a few samples.

## OCCURRENCE AND TEXTURES OF APATITE

Observations of undisturbed samples in thin section (OM) and in natural loose fragments (SEM-EDS) allowed us to identify three major groups of apatite, in which we recognize seven variants (types 1 to 7).

In the first group, the grains are ovoid to prismatic, occurring in isolation or in assemblages with a mosaic texture. In the second group, we distinguish: a) borders (overgrowths) with a higher birefringence, b) intra-crystalline bands (replacive veins with a seam in the middle), c) tiny tabular prismatic crystals, and d) borders with a lamellar habit. The third group is found, in general, in a fissured medium, deposited in discontinuities but also as secondary aggregates formed during remobilization processes, constituting an unstructured mass without any geometrical heritage from the original material. In this group, we distinguish fibrous apatite in fibroradial aggregates, and globular (spherulitic) aggregates; the first one (fibrous) differs from the globular type because of the larger dimension of the crystals, and because the external surface of the aggregates does not form a complete and perfect spherulite. Their morphology on a microscopic scale is described below.

### *First group (types 1, 1a)*

The ovoid apatite from this group is found throughout the whole weathering profile, from the fresh rock to soil. It displays evidence of weathering in samples from the intermediate and upper levels of the profile. In fresh rock, it occurs mainly disseminated or as concentrations (apatite) within the carbonatite and, in lower concentrations, in the alkaline silicate rocks. The grains are commonly either ovoid (Fig. 3a) or almost prismatic, rarely euhedral, and in general, with a mosaic texture. There are great variations in grain size, with dimensions of 0.01 mm to 0.1 mm long being the common range, and coarse-grained zones containing grains exceeding 1 mm.

Weathered samples comprise fresh and variably weathered ovoid grains of apatite, presenting signs of textural changes; these crystals are still primary apatite, because of their origin, but they present morphological changes associated with the weathering processes, such as fracturing, dissolution cavities, and changes in color and texture (Figs. 3b, c). Their chemical composition also shows changes in relation to fresh grains, as discussed in the geochemical and crystallographic descriptions below. Thus we distinguish type 1a, corresponding to parts of primary grains of apatite showing chemical changes induced by weathering.

### *Second group (types 2, 3, 4 and 5)*

Types 2 to 5 are present as a restricted transformation of the primary crystals of apatite into the following four morphological types. In type 2, a higher-birefrin-

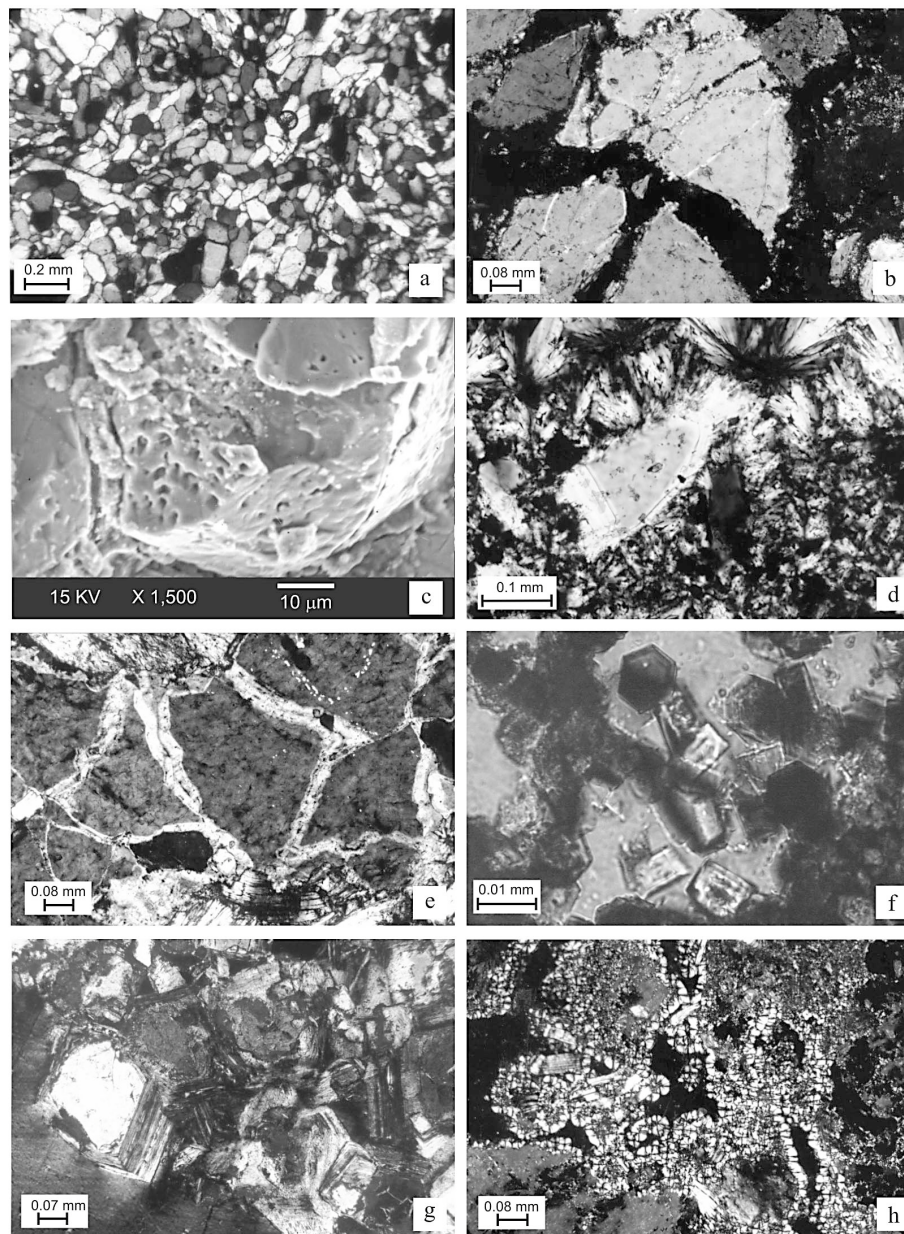


FIG. 3. Photomicrographs of types of apatite at Catalão I. a. Ovoid to prismatic unweathered crystals with a mosaic texture (type 1), occurring as concentrations within the carbonatite (sample 22, 50 m depth, front 1, OM). b. Heterogeneously weathered crystal of apatite (type 1a); such material is still considered primary apatite, because of its origin; it displays color, textural, and morphological changes associated with the weathering processes, such as fracturing and dissolution cavities (sample 35, 41 m depth, front 1, OM). c. Fractured apatite with dissolution-induced porous (type 1a) (sample 35, 40 m depth, front 1, SEM). d. Primary apatite (type 1) with overgrowths along intercrystalline discontinuities around it, whose texture indicates *in situ* growth in optical continuity (type 2), and fibrous supergene apatite (type 6) in fibroradial aggregates (sample 62, 34 m depth, front 1, OM). e. Primary apatite (type 1) with replacive intracrystalline veins of acicular crystals of type-3 apatite (sample 36, 45 m depth, front 1, OM). f. Randomly disposed tiny tabular prismatic crystals of apatite (type 4) (sample 42, 55 m depth, front 1, OM). g. Apatite with lamellar habit (type 5) surrounding primary apatite (type 1) (sample 60, 56 m depth, front 1, OM). h. Supergene apatite occurring mainly as semiglobules, linked to each other in botryoidal growths or in massive assemblages (type 7) (drill hole f58, 147 m depth, OM).

gence border occurs only along intercrystalline discontinuities as an overgrowth around apatite grains of the first group, in a typically authigenic texture indicating *in situ* growth in optical continuity with the core. The thickness of the overgrowth around the apatite core is variable, up to tens of micrometers, or it can make up the whole grain, indicating that this type is not only an overgrowth, but may be also a replacement, in general partial and rarely total, of apatite grains from the first group (Fig. 3d).

In type 3, intracrystalline bands cross grains of primary apatite, mainly along intracrystalline discontinuities in apatite of the first group. The bands are composed of acicular parallel crystals disposed perpendicular to the wall of the host apatite. This type has a higher birefringence than the ovoid apatite. The morphology suggests different conditions of formation in relation to type 2, because type 3 is not in optical continuity with the apatite grains of the first group, which is crossed by these bands, and can be seen as replacive veins (Fig. 3e).

In type 4, aggregates of randomly disposed tabular prismatic crystals of apatite display a common tendency toward idiomorphism; although their dimensions are very reduced (*ca.* 5  $\mu\text{m}$ ), it is possible to see the prismatic hexagonal habit in some sections and their higher birefringence (Fig. 3f). The aggregates of this type can be found either associated with remnants of apatite of the first group, a fact that allowed us to recognize this type as replacing an earlier generation of apatite, or it is devoid of such relict apatite. In both cases, these aggregates do not show any geometric heritage from the prior apatite.

In type 5, borders have a lamellar habit; these are less common than the previous types and occur surrounding grains of primary apatite. Their thickness varies from 0.01 to 0.1 mm, and the borders also present a higher birefringence (Fig. 3g).

#### *Third group (types 6 and 7)*

This group is found in weathered material, in fissures and in aggregates of secondary plasma, forming variably porous assemblages of the following two types. Type 6 consists of fibrous crystals occurring in fibroradial aggregates, perpendicular to the surface of deposition; the formation of more or less continuous botryoidal deposits also is common. The surface of deposition may consist of a trans-, inter-, or intramineral discontinuity in any material, for instance in apatite grains of the first group, with (Fig. 3d) or without overgrowths described above. The fibrous apatite may also constitute a secondary plasma in weakly porous assemblages, locally forming fibroradial rosettes. These assemblages may be considered an example of a crystalliplasma, in the micromorphological terminology of Brewer (1964) and Delvigne (1998) (Fig. 3d). The fibrous supergene apatite has a wider distribution in the

weathering profile than type-7 apatite, which is globular, with a cross-shaped undulatory extinction occurring mainly as incomplete globules or semi-globules, which are linked to each other generally in botryoidal growths or in relatively massive assemblages. The globules may have formed around a tiny differentiated nucleus composed of either a ferruginous accumulation or unrecognized materials that may be associated with apatite fragments or remains of the first group (Fig. 3h). These types occurs mainly in weakly weathered rock.

#### *The three groups*

These three groups are found to be related to a) magmatic, b) postmagmatic or hydrothermal, and c) weathering processes, for the following reasons. Ovoid group-1 (magmatic) apatite is found over the entire profile, from fresh rock to soil samples; in weathered and pedological samples, this type may present signs of textural changes due to typical processes of weathering. This type will be referred as *primary* apatite. Where affected by weathering, but not yet destroyed or dissolved, it may be referred to as weathered. Group-2 apatite, of postmagmatic or hydrothermal origin, forms overgrowths, replacive veins, tiny prismatic crystals, and lamellar borders present mainly in unweathered samples. The higher-birefringence borders (overgrowths) also occur in weathered samples, but never as clearly as in unweathered material. In weathered samples, it presents textural signs of changes due to weathering processes, such as partial dissolution, forming interruptions in morphology seen in fresh samples. This group is referred as *postmagmatic* or *hydrothermal* apatite. Group-3 apatite, of supergene origin, is fibrous and globular; it is found in weathered material, in fissures and within secondary plasma aggregates, forming variably porous assemblages, commonly associated with iron oxides, clearly indicative of their origin by weathering processes. This apatite is referred to as *supergene* apatite. It is worth noting that we use the term "supergene" only in the strict sense, indicating phases or features formed during weathering, and not simply affected by it.

The following sections show that the seven types of apatite, from those three main groups, present some differences in chemical composition and other characteristics, allowing us to discriminate the geochemical trends among the three groups, including changes in magmatic apatite affected by weathering.

#### CATHODOLUMINESCENCE (CL)

The various types of apatite, except for type 4 (replacive intracrystalline veins), were studied by optical microscopy coupled with cathodoluminescence. Using CL colors, activated by elements such as the REE and Mn, minor differences in their contents, not detectable by electron microprobe, may be observed. Activa-

tion spectra were not used to identify the elements responsible.

The unaltered and unweathered grains of primary apatite from Catalão I have a blue-violet luminescence. According to Marshall (1988), the violet color characterizes primary apatite from carbonatite and is due to the presence and distribution of Dy and  $\text{Eu}^{2+}$ . Mitchell *et al.* (1997) studied CL spectra from synthetic fluorapatite doped with individual rare-earth-element activators, and concluded that more research is needed to interpret the CL spectra of natural apatite, because these result from the subtle interplay of major factors (the relative concentrations of the individual REE, their relative efficiency in promoting luminescence, and the presence or absence of elements that may act as activators, suppressors or co-enhancers of CL).

The CL images from primary apatite grains affected by weathering (type 1a) display the blue-violet color in the fresh regions of the crystals, and different colors near discontinuities. This fact suggests the importance of chemical changes in these parts of the grains, where they are affected by chemical weathering but not still dissolved; this point will be discussed later, with chemical data. The CL images of apatite overgrowths (type 2) forming higher-birefringence borders around primary apatite grains, display luminescence colors similar to the blue-violet of the primary apatite, probably indicating the presence of the same activator elements. The tabular prismatic crystals of apatite (type 4) display a heterogeneous luminescence: blue-violet, blue, and yellow. According to Marshall (1988), Mn is the main activator of the yellow luminescence in hydrothermal apatite. The lamellar apatite (type 5) does not display CL activation.

Neither type of supergene apatite (fibrous and globular) displays luminescence colors. The observed lack of luminescence for some types of apatite (5, 6, and 7) may result from the distribution and combination of the activator elements, and does not necessarily mean that they are lacking in these activator elements (*e.g.*, the light REE and Mn).

#### GEOCHEMICAL AND CRYSTALLOCHEMICAL FEATURES

##### Unit-cell parameters

Calculations of the unit-cell parameters by the least-squares method (software LCLSQ8) were made from XRD spectra of samples of each morphological type of apatite. Calculated values are presented in Table 1, along with values obtained by Lenharo (1994) using the same method, but on bulk concentrates from Catalão I (*i.e.*, mixed types). Two of the apatite concentrates prepared and analyzed by Lenharo (1994) were analyzed again and used as a reference. The new values are quite similar to the old ones.

Samples of primary apatite (CAF22 and CAF27) present similar values to those obtained by Lenharo (1994), in which *a* and *c* values are larger than the ref-

erence JCPDS fluorapatite. These higher values could be due to the presence of  $\text{OH}^-$  located in the channels and the high amount of Sr in the cationic position. Table 1 includes data of Pereira (1995) and Pereira *et al.* (1997) for Catalão I primary apatite.

##### Raman micro-spectroscopy

Determination of anionic content in apatite is very important because the substitutions in the anionic sites are coupled with other elements to ensure electro-neutrality. The evaluation of the proportion of  $\text{CO}_3^{2-}$ , which substitutes for  $\text{PO}_4^{3-}$ , by simple difference in the calculated structural formula is generally found in the literature (*e.g.*, Le Bas & Handley 1979).

In this work, some samples were analyzed with Raman microspectrometry (RM), in order to obtain information about the content and crystallochemical position of the  $\text{CO}_3^{2-}$ . Although there is a vast bibliography about the application of Raman spectroscopy in synthetic and biological apatite materials, there are no references applied to minerals. Polarization studies as recommended by Tsuda & Arends (1994) have not been carried out on minerals.

Boulingui (1997) used the method of Nelson & Williamson (1982), Mul *et al.* (1986, 1988) and Beny *et al.* (1996) in applying this technique to powdered apa-

TABLE 1. CALCULATED UNIT-CELL PARAMETERS OF PRIMARY APATITE FROM THE CATALÃO I CARBONATITE, BRAZIL, COMPARED WITH VALUES OBTAINED BY LENHARO (1994)

Sample	<i>a</i> (Å)	<i>c</i> (Å)	Volume (Å <sup>3</sup> )
CAF22	9.398 (1)	6.902 (2)	527.9 (2)
CAF27	9.394 (1)	6.893 (2)	526.9 (2)
CAMC1	9.393 (1)	6.896 (1)	526.8 (1)
CAMC1 (L)	9.3906	6.8920	529.37
CAMM15	9.392 (1)	6.891 (2)	526.4 (2)
CAMM15 (L)	9.3934	6.8918	526.52
CAMM5	9.399 (1)	6.892 (1)	527.3 (1)
CAMM5 (L)	9.3971	6.8914	527.01
CAMS3	9.364 (1)	6.903 (1)	524.1 (1)
CAMS3 (L)	9.3499	6.8956	522.05

Reference materials	<i>a</i> (Å)	<i>c</i> (Å)
Fluorapatite JCPDS 15-876	9.3684	6.8841
Fluorapatite from Durango (Young <i>et al.</i> 1969)	9.391	6.878
Fluorapatite (McClellan & Lehr 1969)	9.377	6.886
Fluorapatite (Winchell 1951, Larsen <i>et al.</i> 1952)	9.38	6.89
Hydroxyapatite JCPDS 9-432	9.418	6.884
Chloroapatite JCPDS 24-0214	9.598	6.776
Chloroapatite JCPDS 33-271	9.641	6.771
Carbonate-fluorapatite JCPDS 19-272	9.309	6.927
Type-B carbonate-apatite (L)	9.36	6.89
Carbonate-fluorapatite JCPDS 31-267	9.346	6.887
Carbonate-fluorapatite (McClellan & Lehr 1969)	9.322	6.900
Strontium-apatite JCPDS 33-1348	9.766	7.276
Strontium-fluorapatite (Larsen <i>et al.</i> 1952)	9.41	6.91
Strontium-hydroxyl-fluorapatite without $\text{CO}_3^{2-}$ (L)	9.3934	6.8908
Carbonate-fluorapatite without $\text{OH}^-$ (L)	9.3558	6.8798

(L): Lenharo (1997).

tite from carbonatite; this type of sample preparation (powder) does not need polarization studies, but does not allow the type control of the analyzed apatite.

Nelson & Williamson (1982) and Mul *et al.* (1988) used the width at half-height of the  $965\text{ cm}^{-1}$  peak for the calculation of the degree of carbonate incorporation in synthetic and biological apatite. They found a direct relation between this width and  $\text{CO}_3^{2-}$  content, and the degree of crystallinity of the apatite. This approach has been criticized because incorporation of the carbonate anion into the apatite structure is not the only factor causing a decrease in its crystallinity.

Leroy (1997) and Penel *et al.* (1998) developed a method of calculation based on the intensity variation and the displacement of peaks corresponding to C–O and P–O bonds, which are associated with the amount of  $\text{CO}_3^{2-}$  present at the *Y* site. This type of carbonate incorporation is particularly evident through the displacement of the  $1078\text{ cm}^{-1}$  peak to  $1070\text{ cm}^{-1}$ . The research was applied to synthetic and biological apatite-group phases so fine-grained that polarization studies were not required. In oriented crystals, according to Tsuda & Arends (1994), variations in intensity, and in some cases, in position of the peaks, occur owing to: 1) the crystal positions in relation to the polarization direction of the laser that reaches the sample, 2) the polarization direction of the Raman re-emission, and 3) the position of the *c* axis in the analyzed crystal, *i.e.*, whether it is precisely parallel to the thin section studied.

This method was applied to the Catalão I materials. Crystals of known morphological and geochemical type were selected with the *c* axis parallel to the section. Each crystal was measured in three positions ( $0^\circ$ ,  $45^\circ$ , and  $90^\circ$ ) related to polarization directions of the laser and of the Raman re-emission, both parallel to each other. Accurate calculations were made only on crystals with a sufficiently controlled orientation.

The calculation according to Penel *et al.* (1998) and Leroy (1997) and the results obtained allowed us to confirm the  $\text{CO}_3^{2-}$  position in its substitution for  $\text{PO}_4^{3-}$  (type *B*). The results from Raman spectra were also compared with the values calculated by difference in the structural formula (electron microprobe).

The values from RM spectra (Table 4) were found to be similar to those calculated by difference, thus validating the method of calculation and the quality of the electron-microprobe data. The values obtained vary from zero (primary apatite) to 7 wt.%  $\text{CO}_3^{2-}$  (some examples of supergene apatite), which is equivalent to about 0.8  $\text{CO}_3^{2-}$  in the double formula of apatite. As mentioned above, some morphological types could not be analyzed because oriented crystals, with their *c* axis parallel to the section, were not found in the thin sections available.

In the RM study, some apatite grains display the simultaneous presence of carbonate incorporation and carbonate absence ( $1070$  and  $1078\text{ cm}^{-1}$  peaks, respectively), which may be interpreted as a compositional heterogeneity on a very small scale, *i.e.*, within the

micrometer volume reached by the laser beam. The required evaluation of the  $\text{OH}^-$  content was not possible owing to poor precision on peak position in the corresponding region of the RM spectrum ( $3400\text{--}3500\text{ cm}^{-1}$ ).

#### *Fourier-transform infrared spectroscopy and differential thermal and thermogravimetric analysis*

Fourier-transform infrared spectroscopy (FTIR) and differential thermal and thermogravimetric analysis (DTA–TGA) were used to verify the anionic content in single-phase primary samples. DTA–TGA analyses did not display the expected mass-loss for the analyzed samples of primary apatite, which would be equivalent to  $\text{CO}_3^{2-}$  plus  $\text{OH}^-$ . The result may be interpreted as a lack of detection by the equipment, since the presence of some of these anionic groups was suggested by other techniques.

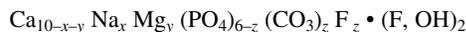
FTIR analysis display very inconspicuous peaks for both anionic groups. The calculation for  $\text{CO}_2$  using the method of Lehr *et al.* (1968) and Scheib *et al.* (1984) results in values around 0.06 wt.%, *i.e.*, close to zero. For the hydroxyl ion, the calculation was not possible.

#### *Electron-microprobe data*

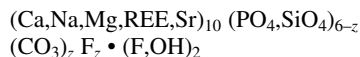
The number of analyzed points in our program of electron-microprobe (EMP) analyses varied according to the observed heterogeneity of each type of apatite. A summary of results for apatite types 1 to 7, with minimum, middle and maximum values of constituents, are shown in Table 2. Chlorine was sought but not found.

Analyses of primary apatite with totals higher than 98% were considered as primary apatite of type 1, whereas apatite whose analytical totals are below this value were classified as type 1a, corresponding to crystals of primary apatite affected by weathering, with some geochemical changes.

These data were used for the calculations of structural formulae. Considering all the problems pointed out in these calculations in the section on Background Information, we have taken the general formula established by McArthur (1990), modified from McClellan (1980), because of the relation between excess  $\text{F}^-$  and the amount of  $\text{CO}_3^{2-}$  substituting for  $\text{PO}_4^{3-}$ :



We also added  $\text{SiO}_4^{4-}$  to the *X* site, and Sr and REE to the *A* site to obtain the general formula:



This formula takes into account the following features: 1)  $\text{OH}^-$  is considered, which is not always the case in the literature, 2)  $\text{SiO}_4^{4-}$  is not necessarily linked to

charge compensation in view of the substitution of  $\text{CO}_3^{2-}$  for  $\text{PO}_4^{3-}$ , and 3) it allows distribution of  $\text{F}^-$  between the channels (with  $\text{OH}^-$ ) and in association with  $\text{CO}_3^{2-}$  in the ratio 1:1, as supported by the majority of investigators.

Concerning the latter point, Table 3 shows amounts of  $\text{OH}^-$  and the corresponding weight percentages for the three hypotheses: (a) all the  $\text{F}^-$  is in the channels, (b)  $\text{F}^-$  not in the channels /  $\text{CO}_3^{2-} = 0.4/1$ , *i.e.*, only 40% of the carbonate substituting for  $\text{PO}_4^{3-}$  would be followed

by  $\text{F}^-$  out of the channels, and (c)  $\text{F}^-$  not in the channels /  $\text{CO}_3^{2-} = 1/1$ , *i.e.*, all the carbonate substituting for  $\text{PO}_4^{3-}$  would be accompanied by an equivalent amount of  $\text{F}^-$ . In these calculations, it can be seen that the molecular weight does not change significantly, as the hydroxyl is a very light ion.

Table 3 also includes the stoichiometric coefficient of C in the formula and the corresponding  $\text{CO}_2$  contents (wt.%) to compare with the values determined by RM, in the cases where this determination was possible (Table 4).

TABLE 2. CHEMICAL COMPOSITION OF APATITE, TYPES 1 TO 7, FROM THE CATALÃO I CARBONATITE, BRAZIL

	F	Na <sub>2</sub> O	MgO	SiO <sub>2</sub>	P <sub>2</sub> O <sub>5</sub>	CaO	MnO	SrO	BaO	La <sub>2</sub> O <sub>3</sub>	Ce <sub>2</sub> O <sub>3</sub>	O=F	total	CaO / P <sub>2</sub> O <sub>5</sub>	REE <sub>2</sub> O <sub>3</sub>	F / P <sub>2</sub> O <sub>5</sub>	
1 n=36	mean	2.39	0.18	0.00	0.23	41.28	54.11	0.04	1.24	0.00	0.14	0.55	1.00	99.15	1.31	0.70	0.06
	min.	1.84	0.01	0.00	0.00	40.07	52.06	0.00	0.72	0.00	0.00	0.00	0.78	98.06	1.26	0.00	0.05
	>98% max.	3.03	0.61	0.00	0.84	42.05	54.99	0.16	2.27	0.00	0.77	1.44	1.28	100.06	1.37	2.21	0.08
1a n=18	mean	2.72	0.16	0.03	0.12	39.34	52.89	0.05	1.78	0.00	0.12	0.44	1.15	96.50	1.35	0.56	0.07
	min.	1.99	0.00	0.00	0.00	35.39	48.92	0.00	0.60	0.00	0.00	0.00	0.84	92.42	1.28	0.00	0.05
	<98% max.	3.81	0.33	0.23	0.50	41.07	54.94	0.17	6.15	0.00	0.35	0.98	1.60	97.99	1.55	1.12	0.10
2 n=6	mean	3.15	0.02	0.14	0.06	36.61	54.71	0.02	0.44	0.00	0.00	0.00	1.33	93.83	1.50	0.00	0.09
	min.	2.81	0.00	0.00	0.00	35.12	53.50	0.00	0.00	0.00	0.00	0.00	1.18	92.11	1.44	0.00	0.08
	max.	3.65	0.06	0.32	0.21	38.87	55.83	0.12	0.58	0.00	0.00	0.00	1.54	96.81	1.55	0.00	0.09
3 n=7	mean	3.40	0.09	0.06	0.00	37.88	52.66	0.04	1.91	0.31	0.00	0.13	1.43	95.10	1.39	0.13	0.09
	min.	2.27	0.00	0.00	0.00	35.80	45.95	0.00	0.00	0.00	0.00	0.00	0.96	86.42	1.28	0.00	0.06
	max.	3.92	0.16	0.22	0.00	39.36	56.64	0.09	3.94	2.14	0.00	0.54	1.65	98.39	1.46	0.54	0.10
4 n=8	mean	3.45	0.20	0.09	0.29	36.10	50.30	0.08	5.84	0.00	0.12	0.48	1.45	95.49	1.39	0.60	0.10
	min.	3.11	0.08	0.00	0.00	33.39	46.74	0.02	2.67	0.00	0.00	0.00	1.31	93.45	1.33	0.00	0.08
	max.	3.79	0.32	0.20	1.00	38.49	53.93	0.20	11.06	0.00	0.39	1.08	1.60	97.32	1.49	1.35	0.11
5 n=8	mean	3.54	0.01	0.00	0.06	39.87	56.04	0.03	0.11	0.00	0.00	0.00	1.49	98.16	1.41	0.00	0.09
	min.	3.37	0.00	0.00	0.00	37.25	53.42	0.00	0.00	0.00	0.00	0.00	1.42	93.58	1.36	0.00	0.08
	max.	3.81	0.02	0.00	0.26	40.84	57.46	0.07	0.46	0.00	0.00	0.00	1.60	100.43	1.44	0.00	0.10
6 n=9	mean	3.16	0.00	0.07	0.07	37.02	54.01	0.04	0.48	0.04	0.00	0.00	1.33	93.56	1.46	0.00	0.09
	min.	2.75	0.00	0.00	0.00	35.56	53.48	0.00	0.36	0.00	0.00	0.00	1.16	92.10	1.41	0.00	0.08
	max.	3.51	0.00	0.26	0.25	38.04	55.60	0.14	0.58	0.37	0.00	0.00	1.48	95.37	1.51	0.00	0.09
7 n=14	mean	2.98	0.00	0.48	0.12	34.94	53.10	0.03	0.52	0.53	0.00	0.00	1.25	91.62	1.52	0.00	0.09
	min.	2.76	0.00	0.26	0.00	33.41	49.92	0.00	0.36	0.36	0.00	0.00	1.16	87.76	1.40	0.00	0.08
	max.	3.36	0.00	0.75	0.40	37.49	55.63	0.11	0.87	0.84	0.00	0.00	1.42	93.97	1.62	0.00	0.10
8		2.33	0.00	0.00	0.49	38.84	54.21	0.00	0.83	0.00	0.00	0.50	0.98	96.22	1.40	0.50	0.06
		2.16	0.00	0.00	0.73	39.31	54.65	0.05	0.84	0.00	0.29	0.68	0.91	97.80	1.39	0.97	0.06
		2.36	0.12	0.00	0.62	40.53	54.70	0.00	0.70	0.00	0.44	0.62	0.99	99.10	1.35	1.06	0.06
		3.94	0.18	0.00	0.22	35.10	51.52	0.00	0.00	0.00	0.00	0.00	1.66	89.30	1.47	0.00	0.11
		3.56	0.00	0.00	0.00	36.73	53.78	0.00	0.34	0.00	0.00	0.00	1.50	92.91	1.46	0.00	0.10
		2.80	0.00	0.00	0.00	35.89	53.19	0.00	0.44	0.00	0.00	0.00	1.18	91.14	1.48	0.00	0.08
		2.66	0.18	0.00	0.62	39.07	54.01	0.00	0.79	0.00	0.33	0.89	1.12	97.43	1.38	1.22	0.07
		2.55	0.14	0.00	0.51	40.19	54.49	0.00	0.76	0.00	0.37	0.65	1.07	98.59	1.36	1.02	0.06
		3.31	0.00	0.00	0.00	35.64	52.39	0.08	0.36	0.00	0.00	0.00	1.39	91.03	1.47	0.00	0.09
		2.88	0.00	0.00	0.00	33.26	48.48	0.00	0.32	0.00	0.00	0.84	1.21	87.76	1.46	0.84	0.09

Definition of the types of apatite: (1) Primary magmatic apatite, fresh grains (total > 98%). (1a): weathered grains (total < 98%). Hydrothermal or postmagmatic-alteration-induced apatite: (2) Overgrowths, (3) Intracrystalline bands (replacive veins), (4) Tiny tabular prismatic crystals, and (5) Borders with a lamellar habit. Supergene apatite: (6) Fibroradial aggregates, and (7) Globular apatite. Weathering of a single grain: (8). The data were obtained with an electron microprobe and are summarized by showing the mean, minimum and maximum values, expressed in wt.%.

THE COMPOSITIONAL VARIABILITY OF THE DIFFERENT TYPES OF APATITE IN CATALÃO I

Results displaying the compositional variability of different groups of apatite are given in Tables 2, 3 and 4. The complete results of original analyses (1999) are available from the Depository of Unpublished Data, CISTI, National Research Council of Canada, Ottawa, Ontario K1A 0S2, Canada.

In Tables 2 and 3, the compositions are represented only by the averages, minimum, and maximum values. Table 4 shows the average structural formula for the various types of apatite as well as their OH<sup>-</sup> and CO<sub>2</sub>

contents found by difference in the calculation of the formula, the CO<sub>2</sub> contents calculated by Raman spectra, and the CaO/P<sub>2</sub>O<sub>5</sub> value. Hence, this table allows a comparison among the seven types of apatite at Catalão I using the main geochemical parameters.

Figures 4 and 5 are binary plots of several geochemical parameters and chemical elements present in apatite grains from types 1 to 7. These are expressed as the number of atoms per formula unit (*apfu*). In Figure 4, we present data for all types of apatite, whereas in Figure 5, we present the compositions in one single grain of apatite, which is partially and heterogeneously weathered (type 1a, Fig. 3b).

TABLE 3. STRUCTURAL FORMULAE OF APATITE, TYPES 1 TO 7, FROM THE CATALÃO I CARBONATITE, BRAZIL

		F	Na	Mg	Si	P	Ca	Mn	Sr	Ba	La	Ce	C(calc.)	OHa	OHb	OHc	MWa	MWb	MWc	CO <sub>2c</sub>
1	mean	1.273	0.058	0.000	0.039	5.895	9.778	0.005	0.121	0.000	0.008	0.030	0.071	0.727	0.755	0.798	1014	1018	1019	0.306
	min.	0.976	0.002	0.000	0.000	5.691	9.560	0.000	0.070	0.000	0.000	0.000	0.000	0.378	0.445	0.454	1006	1018	1018	0.000
	max.	1.622	0.203	0.000	0.143	6.013	9.878	0.023	0.225	0.000	0.042	0.079	0.288	1.024	1.122	1.269	1024	1020	1023	1.240
1a	mean	1.480	0.053	0.008	0.020	5.716	9.724	0.007	0.177	0.000	0.007	0.024	0.265	0.520	0.626	0.785	1009	1020	1022	1.135
	min.	1.073	0.001	0.000	0.000	5.040	9.185	0.000	0.059	0.000	0.000	0.000	0.000	0.070	0.319	0.319	977	1018	1018	0.000
	max.	2.112	0.110	0.059	0.085	5.989	9.937	0.025	0.625	0.000	0.019	0.055	0.960	0.927	0.975	1.307	1026	1025	1034	4.080
2	mean	1.684	0.006	0.035	0.010	5.241	9.913	0.004	0.043	0.000	0.000	0.000	0.749	0.317	0.616	1.065	984	1023	1031	3.193
	min.	1.476	0.000	0.000	0.000	5.029	9.854	0.000	0.000	0.000	0.000	0.000	0.499	0.070	0.269	0.569	975	1021	1026	2.140
	max.	1.930	0.018	0.080	0.036	5.501	10.000	0.017	0.058	0.000	0.000	0.000	0.971	0.524	0.857	1.379	991	1025	1035	4.130
3	mean	1.847	0.029	0.015	0.000	5.536	9.720	0.005	0.189	0.024	0.000	0.008	0.464	0.153	0.339	0.617	1004	1021	1026	1.986
	min.	1.416	0.000	0.000	0.000	5.291	9.504	0.000	0.000	0.000	0.000	0.000	0.024	0.000	0.124	0.339	989	1018	1018	0.100
	max.	2.070	0.051	0.056	0.000	5.976	9.984	0.013	0.382	0.165	0.000	0.034	0.709	0.584	0.593	0.787	1030	1023	1030	3.030
4	mean	1.878	0.066	0.024	0.051	5.264	9.279	0.012	0.586	0.000	0.007	0.027	0.685	0.122	0.396	0.807	1014	1023	1030	2.925
	min.	1.650	0.027	0.000	0.000	4.841	8.718	0.003	0.260	0.000	0.000	0.000	0.368	0.000	0.238	0.480	999	1021	1024	1.580
	max.	2.057	0.106	0.052	0.174	5.464	9.689	0.029	1.117	0.000	0.021	0.062	1.099	0.350	0.673	1.333	1031	1025	1037	4.670
5	mean	1.865	0.002	0.001	0.009	5.612	9.983	0.004	0.011	0.000	0.000	0.000	0.378	0.135	0.286	0.513	996	1021	1024	1.625
	min.	1.744	0.000	0.000	0.000	5.477	9.941	0.000	0.000	0.000	0.000	0.000	0.174	0.000	0.103	0.227	991	1019	1021	0.750
	max.	2.093	0.007	0.001	0.044	5.783	9.998	0.010	0.046	0.000	0.000	0.000	0.511	0.256	0.426	0.684	1005	1021	1027	2.190
6	mean	1.713	0.000	0.019	0.012	5.375	9.924	0.006	0.048	0.003	0.000	0.000	0.613	0.287	0.532	0.900	989	1022	1028	2.624
	min.	1.484	0.000	0.000	0.000	5.181	9.878	0.000	0.035	0.000	0.000	0.000	0.419	0.091	0.318	0.659	984	1021	1025	1.800
	max.	1.909	0.001	0.066	0.043	5.581	9.954	0.020	0.058	0.025	0.000	0.000	0.819	0.516	0.794	1.213	996	1024	1032	3.490
7	mean	1.617	0.000	0.122	0.021	5.077	9.760	0.005	0.052	0.036	0.000	0.000	0.902	0.383	0.744	1.285	981	1024	1033	3.838
	min.	1.526	0.000	0.068	0.000	4.796	9.674	0.000	0.037	0.023	0.000	0.000	0.543	0.122	0.458	0.962	970	1022	1027	2.330
	max.	1.878	0.000	0.197	0.069	5.457	9.854	0.015	0.087	0.056	0.000	0.000	1.174	0.474	0.930	1.635	995	1026	1038	4.980
8		1.255	0.000	0.000	0.083	5.599	9.891	0.000	0.082	0.000	0.000	0.027	0.317	0.745	0.872	1.062	1003	1020	1023	1.36
		1.150	0.000	0.000	0.123	5.603	9.859	0.007	0.082	0.000	0.016	0.037	0.274	0.850	0.959	1.124	1007	1020	1023	1.18
		1.253	0.039	0.000	0.104	5.758	9.836	0.000	0.068	0.000	0.024	0.033	0.138	0.747	0.802	0.885	1011	1019	1020	0.59
		2.244	0.063	0.000	0.040	5.349	9.937	0.000	0.000	0.000	0.000	0.000	0.611	0.000	0.001	0.367	987	1022	1028	2.61
		1.948	0.000	0.000	0.000	5.378	9.966	0.000	0.034	0.000	0.000	0.000	0.622	0.052	0.301	0.674	989	1022	1029	2.66
		1.547	0.000	0.000	0.000	5.308	9.955	0.000	0.045	0.000	0.000	0.000	0.692	0.453	0.730	1.145	986	1023	1030	2.96
		1.425	0.059	0.000	0.105	5.600	9.797	0.000	0.078	0.000	0.018	0.048	0.295	0.575	0.693	0.871	1006	1020	1023	1.27
		1.358	0.046	0.000	0.086	5.726	9.825	0.000	0.074	0.000	0.020	0.035	0.188	0.642	0.718	0.831	1009	1019	1021	0.81
		1.839	0.000	0.000	0.000	5.299	9.857	0.012	0.037	0.000	0.000	0.000	0.701	0.161	0.442	0.863	988	1023	1030	3.00
		1.655	0.000	0.000	0.000	5.114	9.433	0.000	0.034	0.000	0.000	0.049	0.886	0.345	0.700	1.232	991	1024	1033	3.78

Definition of the types of apatite: (1) Primary magmatic apatite, fresh grains (total > 98%). (1a): weathered grains (total < 98%). Hydrothermal or postmagmatic-alteration-induced apatite: (2) Overgrowths, (3) Intracrystalline bands (replacive veins), (4) Tiny tabular prismatic crystals, and (5) Borders with a lamellar habit. Supergene apatite: (6) Fibroradial aggregates, and (7) Globular apatite. Weathering of a single grain: (8). The data were obtained with an electron microprobe and are summarized by showing the mean, minimum and maximum values, expressed in atoms per formula unit. The structural formulae are calculated on the basis of 10 cations per formula unit. OHa, OHb, OHc, MWa, MWb, and MWc are results of different calculations of OH and molecular weight: (a) all F<sup>-</sup> within the structural channels, (b) F<sup>-</sup> outside the channels / CO<sub>3</sub><sup>2-</sup> = 0.4 / 1, and (c) F<sup>-</sup> outside the channels / CO<sub>3</sub><sup>2-</sup> = 1 / 1 (see text).

Primary apatite (type 1)

The results indicate the presence of one type of primary apatite with 1.8 to 3 wt.% F, up to 1.3 wt.% REE<sub>2</sub>O<sub>3</sub>, 0.7 to 2.3 wt.% SrO, CO<sub>3</sub><sup>2-</sup> practically absent, very low OH<sup>-</sup> (evaluated only by difference in calculation), CaO/P<sub>2</sub>O<sub>5</sub> value from 1.26 to 1.37, and F/P<sub>2</sub>O<sub>5</sub> value from 0.05 to 0.08. The SiO<sub>2</sub> content varies from 0 to 0.84 wt.%. The constituents Na<sub>2</sub>O, MgO, BaO, Al<sub>2</sub>O<sub>3</sub>, FeO and MnO are invariably lower than the detection limits. The La<sub>2</sub>O<sub>3</sub> and Ce<sub>2</sub>O<sub>3</sub> contents vary from

0 to 0.77 wt.% and from 0 to 1.44 wt.%, respectively. The representative structural formula of this type is: Ca<sub>9.74</sub> Sr<sub>0.18</sub> La<sub>0.02</sub> Ce<sub>0.06</sub> (PO<sub>4</sub>)<sub>6.00</sub> (F<sub>1.47</sub> OH<sub>0.53</sub>), and the proper name is fluorapatite. In previous studies on apatite concentrates of the same area, Lenharo (1994) also documented one type as primary apatite, and classified it as “strontium-hydroxy-fluorapatite”, in which the hydroxyl was verified by FTIR. Pereira (1995) also found significant values of Sr in primary apatite from this area, in addition to high fluorine and low and variable CO<sub>3</sub><sup>2-</sup> content.

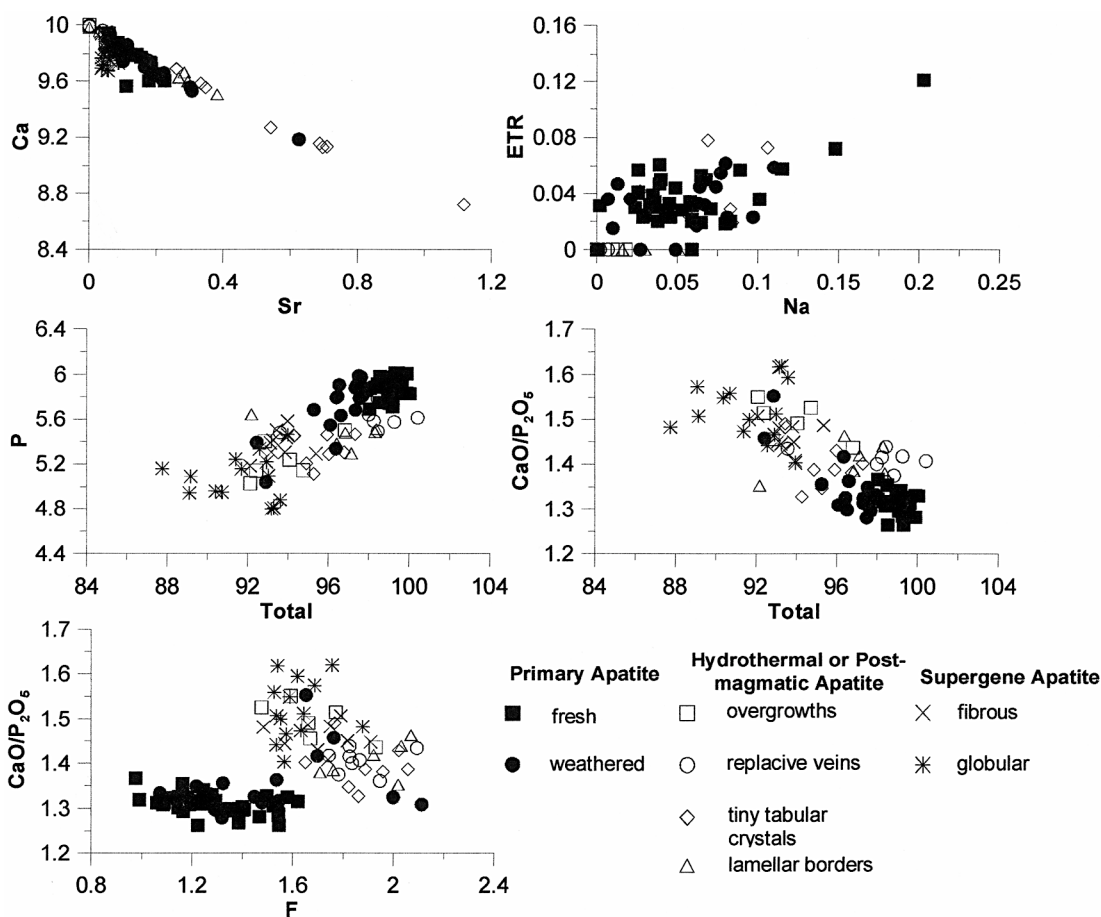


FIG. 4. Binary plots correlating geochemical parameters and chemical elements present in apatite, expressed by number of atoms per formula unit of 10 A-site cations, including the ratio CaO/P<sub>2</sub>O<sub>5</sub> and the analytical total of the electron-microprobe analysis, using all obtained and selected data. The geochemical trends from fresh primary apatite to weathered apatite, and to supergene apatite seen in the plots are: loss of cations that substitute for Ca (REE, Na, and Sr), an increase in the ratio CaO/P<sub>2</sub>O<sub>5</sub>, i.e., increase in CO<sub>3</sub><sup>2-</sup> that substitutes for PO<sub>4</sub><sup>3-</sup>, and an increase in F. Hydrothermal and postmagmatic types of apatite (2 to 5) are displayed along the same trends, generally in an intermediate position between igneous (type 1) and supergene apatite (types 6 and 7).

Fluorine contents never reach the theoretical values of saturation of its monovalent anionic site, *i.e.*, 2 *apfu*, in the structural formula based on 10 A-site cations, which would correspond to about 3.67 wt.% F. The OH<sup>-</sup> present at this site, although low in content, is established only by difference in the calculation of the formula.

The primary apatite of Catalão I has a composition in the cationic site similar to that of apatite from other bodies of carbonatite described in the literature. However, the composition also has some peculiarities, such as high contents of REE, compared with other Brazilian carbonatites (Ferrari 2000, Ferrari *et al.* 2001). In the primary apatite from Catalão I, the REE contents attain 2.2 wt.% REE<sub>2</sub>O<sub>3</sub>, corresponding to 0.12 *apfu*.

Among the possible cations that substitute for Ca, only the REE, Na, and Sr present significant values. The plots show a variable positive correlation between REE and Na (Fig. 4); this feature is mentioned in the literature as a coupled substitution for Ca that would ensure electrostatic neutrality of the structure (Hughes *et al.* 1991).

#### Weathered primary apatite (type 1a)

Compositions of apatite from fresh samples, type 1 described above, do not have analytical totals lower than

98%. In contrast, residual apatite grains present in the weathered mantle, with variable degrees of weathering, display systematically low totals, for the reasons explained earlier. As a result, the totals of the spot analyses were taken as an index of the degree of weathering at the analyzed point. These compositions with totals less than 98% can be related to: 1) areas with imperfect luster caused by fragmentation of the crystals during the preparation procedure, which is indicative of the beginning of weathering, at least, by physical weathering, 2) porosity promoted by partial dissolution, which is in some cases visible *via* SEM images, and 3) the existence of elements or compounds whose concentrations is not yet established, *e.g.* CO<sub>3</sub><sup>2-</sup> and OH<sup>-</sup>.

The compositions of primary apatite with low totals (type 1a) (Tables 2, 3, Fig. 4) display systematic changes in relation to primary apatite (type 1), such as higher values of F and CaO/P<sub>2</sub>O<sub>5</sub> value, lower amounts of cations replacing Ca (Na, Mg, REE and Sr), and a lower content of Si. These results indicate that weathering has caused incongruent dissolution, which is confirmed by the set of spot analyses on a weathered grain (Figs. 3b, 5). This detailed study showed the same geochemical evolution mentioned in the previous paragraph, considering the results from central points (away from fissures and from texturally modified zones, and similar to the fresh primary apatite) toward points affected by weath-

TABLE 4. TYPICAL STRUCTURAL FORMULA FOR EACH TYPE OF APATITE FOUND IN THE CATALÃO I CARBONATITE, BRAZIL

Structural typical formula	CO <sub>2</sub> calc. wt% this anal.	CO <sub>2</sub> calc. wt% average	CO <sub>2</sub> Raman wt%	CaO/ P <sub>2</sub> O <sub>5</sub>
<b>Primary magmatic apatite</b>				
(1) fresh grains Ca <sub>9.74</sub> Sr <sub>0.18</sub> La <sub>0.02</sub> Ce <sub>0.06</sub> (PO <sub>4</sub> ) <sub>6.00</sub> (F <sub>1.47</sub> OH <sub>0.53</sub> )	0	0.3	0	1.28
(1a) weathered grains (residual) Ca <sub>9.54</sub> Sr <sub>0.06</sub> (PO <sub>4</sub> ) <sub>5.39</sub> (CO <sub>3</sub> ) <sub>0.61</sub> F <sub>0.61</sub> (F <sub>1.15</sub> OH <sub>0.85</sub> )	2.62	1.13	n.a.	1.46
<b>Hydrothermal or postmagmatic apatite</b>				
(2) overgrowths (borders with higher birefringence) Ca <sub>9.94</sub> Sr <sub>0.06</sub> (PO <sub>4</sub> ) <sub>5.40</sub> (CO <sub>3</sub> ) <sub>0.60</sub> F <sub>0.60</sub> (F <sub>1.07</sub> OH <sub>0.93</sub> )	2.42	3.19	3–4	1.46
(3) replacive intracrystalline veins Ca <sub>9.96</sub> Sr <sub>0.03</sub> (PO <sub>4</sub> ) <sub>5.38</sub> (CO <sub>3</sub> ) <sub>0.62</sub> F <sub>0.62</sub> (F <sub>1.45</sub> OH <sub>0.55</sub> )	2.66	1.99	n.a.	1.46
(4) tiny tabular prismatic crystals Ca <sub>9.15</sub> Sr <sub>0.69</sub> La <sub>0.07</sub> Ce <sub>0.06</sub> (PO <sub>4</sub> ) <sub>5.45</sub> (CO <sub>3</sub> ) <sub>0.55</sub> F <sub>0.55</sub> (F <sub>1.31</sub> OH <sub>0.69</sub> )	2.07	2.93	*	1.33
(5) lamellar borders Ca <sub>10</sub> (PO <sub>4</sub> ) <sub>5.64</sub> (CO <sub>3</sub> ) <sub>0.36</sub> F <sub>0.36</sub> (F <sub>1.48</sub> OH <sub>0.52</sub> )	1.55	1.63	n.a.	1.40
<b>Supergene apatite</b>				
(6) fibrous radial aggregates Ca <sub>9.94</sub> Sr <sub>0.04</sub> (PO <sub>4</sub> ) <sub>5.29</sub> (CO <sub>3</sub> ) <sub>0.69</sub> F <sub>0.69</sub> (F <sub>0.97</sub> OH <sub>1.03</sub> )	3.04	2.62	3–5	1.49
(7) globular aggregates Ca <sub>9.84</sub> Sr <sub>0.05</sub> Mg <sub>0.08</sub> Mn <sub>0.01</sub> Ba <sub>0.03</sub> (PO <sub>4</sub> ) <sub>4.88</sub> (CO <sub>3</sub> ) <sub>1.12</sub> F <sub>0.12</sub> (F <sub>0.50</sub> OH <sub>1.50</sub> )	4.75	3.83	***	1.59

CO<sub>2</sub> contents found by difference in formula calculation (basis of 10 cations), CO<sub>2</sub> contents calculated by Raman spectra (for some types), and CaO/P<sub>2</sub>O<sub>5</sub>. \* Weak incorporation of carbon, \*\*\* strong incorporation of carbon.

ering, with textural modification and next to discontinuities. RM results (Table 4) suggest that  $\text{CO}_3^{2-}$  may be incorporated in this weathered apatite, which originally contained no carbonate.

Some high values of Sr found in the weathered grains (type 1a) should not be construed to indicate that the weathering caused an increase in Sr; they may be an effect of heterogeneity in the primary apatite. In fact, in common with other elements that substitute for Ca, Sr also seems to diminish with weathering. A representative structural formula of the weathered zones in igneous apatite is:  $\text{Ca}_{9.94}\text{Sr}_{0.06}(\text{PO}_4)_{5.39}(\text{CO}_3)_{0.61}\text{F}_{0.61}(\text{F}_{1.15}\text{OH}_{0.85})$ .

*Postmagmatic or hydrothermal apatite (types 2 to 5)*

Among the four different hydrothermal or post-magmatic types of apatite, some of their characteristics are in common, whereas others are distinctive according to type. In comparison with the fresh primary apatite, F enrichment, lower totals and lower contents of Na are common. Only in the overgrowth borders (type 2), in which the presence of  $\text{CO}_2$  was evaluated using RM, were values from 3 to 4 wt.% obtained (Table 4). For the other types (3, 4, and 5), the presence of this anion was established, but not quantified. For apatite of type 4 (tiny prismatic crystals), the amount of  $\text{CO}_2$  is

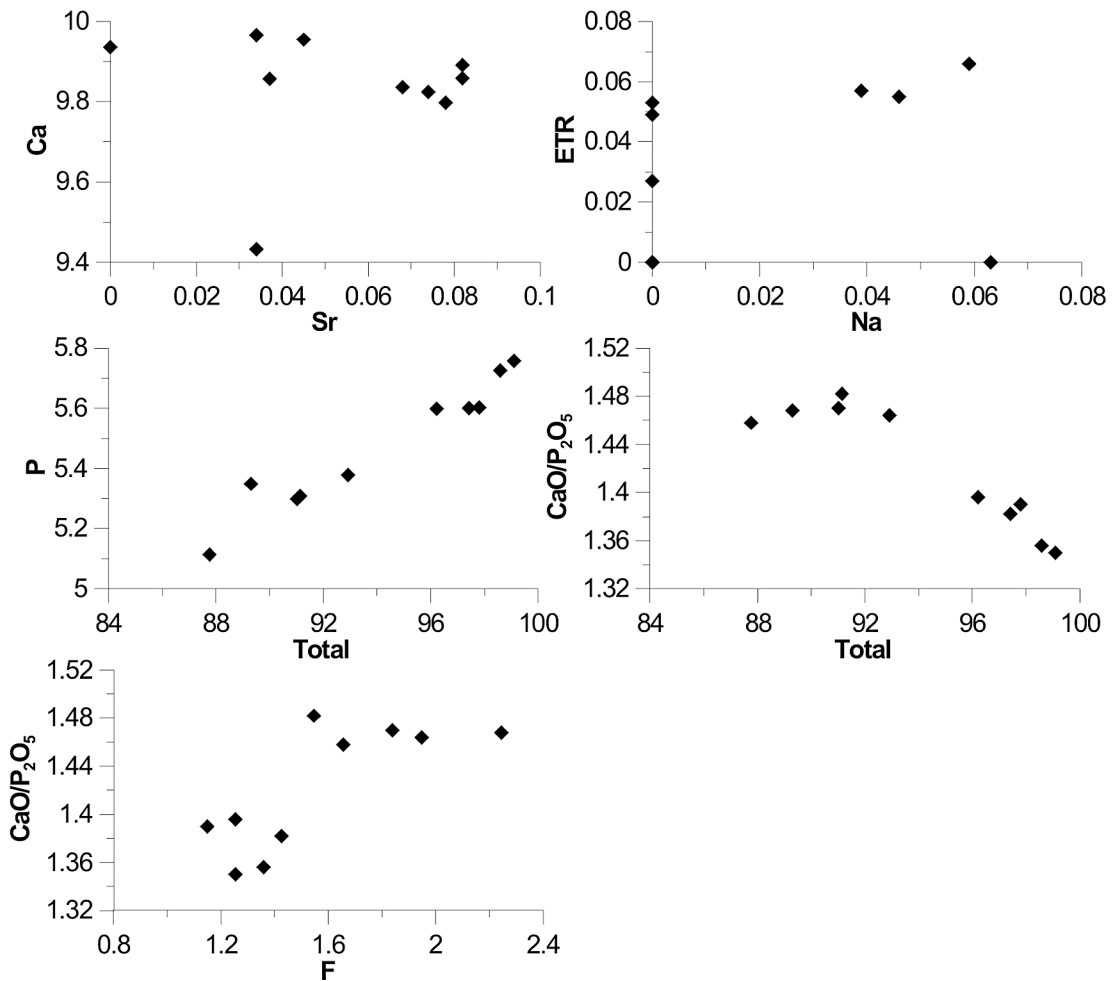


FIG. 5. Binary plots displaying the same correlations as in Figure 4, for spot analyses (also expressed in the number of atoms per formula unit in the structural formula based on 10 A-site cations) in a single apatite grain (Fig. 3b), partially and heterogeneously weathered, displaying the same geochemical trends between igneous and supergene apatite.

low (<1 wt. %). Moreover, these types of apatite present the following peculiarities.

#### *Type 2 (overgrowth borders)*

Among this group (postmagmatic and hydrothermal types), apatite of type 2 has the lowest values of Sr (from below the limit detection to 0.58 wt.% SrO) and the highest CaO/P<sub>2</sub>O<sub>5</sub> ratio (from 1.44 to 1.55). The values of REE<sub>2</sub>O<sub>3</sub> are practically zero. The representative structural formula of type-2 apatite is: Ca<sub>9.94</sub> Sr<sub>0.06</sub> (PO<sub>4</sub>)<sub>5.40</sub> (CO<sub>3</sub>)<sub>0.60</sub> F<sub>0.60</sub> (F<sub>1.07</sub> OH<sub>0.93</sub>).

#### *Type 3 (replacive veins)*

This type has contents of REE<sub>2</sub>O<sub>3</sub> varying from below the limit of detection to about 0.5 wt.% (for Ce<sub>2</sub>O<sub>3</sub>). Sr may be present in relatively high amounts, from below the limit detection to 3.94 wt.% SrO, but it is not as high as in type-4 apatite. The CaO/P<sub>2</sub>O<sub>5</sub> value ranges from 1.28 to 1.46 wt.%. The representative structural formula of this type is: Ca<sub>9.96</sub> Sr<sub>0.03</sub> (PO<sub>4</sub>)<sub>5.38</sub> (CO<sub>3</sub>)<sub>0.62</sub> F<sub>0.62</sub> (F<sub>1.45</sub> OH<sub>0.55</sub>).

#### *Type 4 (tabular tiny prismatic crystals)*

This type displays the highest values of Sr (from 2.7 to 11.1 wt.% SrO) and Na (from 0.08 to 0.32 wt.% Na<sub>2</sub>O). Type-4 apatite has almost similar contents of REE as magmatic apatite (up to 1.4 wt.% REE<sub>2</sub>O<sub>3</sub>). The CaO/P<sub>2</sub>O<sub>5</sub> value varies from 1.33 to 1.49. The representative structural formula of this type is: Ca<sub>9.15</sub> Sr<sub>0.69</sub> La<sub>0.02</sub> Ce<sub>0.06</sub> (PO<sub>4</sub>)<sub>5.45</sub> (CO<sub>3</sub>)<sub>0.55</sub> F<sub>0.55</sub> (F<sub>1.31</sub> OH<sub>0.69</sub>).

#### *Type 5 (lamellar borders)*

As is the case with type 2, lamellar apatite has very low contents of REE, below the limit of detection. Sr varies from below the limit of detection to 0.46 wt.% SrO, and the CaO/P<sub>2</sub>O<sub>5</sub> value varies from 1.36 to 1.44. RM indicates carbonate incorporation amounting to less than 3 wt.% CO<sub>2</sub>. The representative structural formula of this type is: Ca<sub>10</sub> (PO<sub>4</sub>)<sub>5.64</sub> (CO<sub>3</sub>)<sub>0.36</sub> F<sub>0.36</sub> (F<sub>1.48</sub> OH<sub>0.52</sub>).

#### *Supergene apatite (types 6 and 7)*

The supergene types of apatite have low contents of Sr, Na, and REE. Some of their characteristics are similar to those of the types of apatite originating by hydrothermal or postmagmatic processes, including the high F content and the presence of CO<sub>2</sub> [evaluated by RM as being 3 to 5 wt.% in fibrous apatite (type 6) and high, but not quantified, in globular apatite (type 7)]. Consequently, they have lower analytical totals. Moreover, the following features are observed.

#### *Type 6 (fibroradial aggregates)*

Fluorine contents vary from 2.8 to 3.5 wt.%, and Sr contents, from 0.4 to 0.6 wt.%. The CaO/P<sub>2</sub>O<sub>5</sub> value ranges from 1.41 to 1.51. The representative structural formula of this type is: Ca<sub>9.94</sub> Sr<sub>0.04</sub> (PO<sub>4</sub>)<sub>5.29</sub> (CO<sub>3</sub>)<sub>0.69</sub> F<sub>0.69</sub> (F<sub>0.97</sub> OH<sub>1.03</sub>).

#### *Type 7 (globular)*

Fluorine contents vary from 2.76 to 3.36 wt.%, and Sr contents, from 0.36 to 0.87 wt.%. The CaO/P<sub>2</sub>O<sub>5</sub> value reaches the highest values among all types of apatite, from 1.40 to 1.62. Barium and Mg, which are practically absent in the other types of apatite, are relatively enriched in the globular type (up to 0.8 wt.% BaO and 0.8% MgO). This peculiar composition may be related to the former presence of barite in the Mg-rich carbonatites, and to the great depth, in the weathering profile, where globules of this type were found. The representative structural formula of type-7 apatite is: Ca<sub>9.84</sub> Sr<sub>0.05</sub> Mg<sub>0.08</sub> Mn<sub>0.01</sub> Ba<sub>0.03</sub> (PO<sub>4</sub>)<sub>4.88</sub> (CO<sub>3</sub>)<sub>1.12</sub> F<sub>0.12</sub> (F<sub>0.50</sub> OH<sub>1.50</sub>).

#### *General statements*

Some general comments can be made as a result of a comparison of morphologically distinct types of apatite in light of Figures 4 and 5. In these figures, we consider together all types of apatite.

The CaO/P<sub>2</sub>O<sub>5</sub> value increases from the fresh apatite to the weathered apatite and the supergene apatite. This increase is accompanied by a reduction in the analytical total and in the proportion of cations that substitute for Ca (Sr, Na and REE), as verified in Figures 4 and 5. Therefore, this ratio may also be considered as an index of weathering (associated with incorporation type-B carbonate).

The average REE contents does not seem to decrease in the weathered apatite (type 1a: Tables 2, 3, 4). In contrast, the hydrothermal and postmagmatic types of apatite (2, 3 and 5) (overgrowth borders, replacive veins and lamellae, respectively), display low REE contents, whereas type 4 (tabular tiny crystals) shows REE contents similar to the magmatic apatite. Both supergene types of apatite display negligible REE contents.

With respect to the cations that substitute for Ca, Sr is the most important, and ranges from 0.63 *apfu* in the primary apatite to 0.38 in the replacive veins (type 3), whereas the tabular tiny crystals (type 4) present particularly high contents of Sr, up to 1.12 *apfu* at the A site.

## INTERPRETATIONS

*Geochemical trends*

The composition, morphology and crystallochemical features of the igneous apatite, which are monitored in its unit-cell parameters, are similar to the characteristics of apatite from other carbonatitic complexes. It occurs in ovoid grains and has the composition of a Sr-bearing fluorapatite.

During weathering, the primary apatite undergoes internal changes prior to complete dissolution. These internal changes anticipate the geochemical trends presented by supergene apatite, such as a loss of cations that substitute for Ca (total for REE and partial for Sr), an increase in  $\text{CO}_3^{2-}$  that substitutes for  $\text{PO}_4^{3-}$ , and an increase in F. This set of changes may be considered the result of an incongruent dissolution, in the sense of Delmas (1979) and in recent literature concerning apatite (Toledo 1999, Ferrari 2000, Ferrari *et al.* 2001, Costa 2002).

Finally, with the total dissolution of type-1 apatite, P and Ca are released to the medium. Where the conditions are favorable, supergene apatite will precipitate, containing a purer cationic site and some  $\text{CO}_3^{2-}$  substituting for  $\text{PO}_4^{3-}$ . The increase in F is consistent with the mechanism of charge balance due to carbonate incorporation in the phosphate site (Regnier *et al.* 1994). In the weathering profile, where there is an influence of either Al-rich rock types or Al-bearing minerals, the newly formed phosphate is not apatite, but a mineral of the crandallite group (Toledo *et al.* 2002).

The formation of supergene apatite in the weathering profile leads to the fixation of Ca, and to some extent, of Sr. These alkaline-earth elements may be eliminated from the profile in conditions of more evolved weathering, where the supergene apatite is destabilized and part of the P is released, as established in other lateritic mantles in several examples of the Brazilian Amazonian region (Schwab *et al.* 1989), and as displayed in diagrams showing the stability of evolving Al–Ca– $\text{PO}_4$  mineral phases (Vieillard *et al.* 1979). The other cations that substitute for Ca (Na, Mg, and REE) are promptly eliminated during the formation of the fibrous apatite, the most common variety of supergene apatite.

In all hydrothermal and postmagmatic types of apatite, the P contents and the total of the spot analyses are lower than in the primary apatite, whereas the F contents are higher. These characteristics may be associated with  $\text{CO}_3^{2-}$  substitution for  $\text{PO}_4^{3-}$ , coupled with extra stoichiometric F, as pointed out by Regnier *et al.* (1994). In this group, the spot analyses generally indicate a relative enrichment in some of the cations that substitute for Ca (Sr and Mg). The ratio  $\text{CaO}/\text{P}_2\text{O}_5$  is higher in the hydrothermal or postmagmatic types than in primary apatite, reflecting carbonate incorporation in the phosphate site. Because of the rare occurrence of

hydrothermal and postmagmatic apatite in weathered samples, we conclude that these types are more susceptible to weathering.

The evolutionary trends may be summarized either from the primary apatite to some hydrothermal and postmagmatic types and to supergene apatite, or considering the internal changes of type-1 grains of apatite, from the fresh regions to the weathered ones: Si and P decrease (replaced by C), the REE decrease (replaced by Ca), there is an irregular decrease of Sr and Na (replaced by Ca), a decrease in the analytical totals of the spot analyses (increase in non-detectable constituents by EMP: C and OH), an increase in F (coupled with carbonate incorporation), an increase in  $\text{CO}_3^{2-}$  (replacing  $\text{PO}_4^{3-}$ ), an increase in Ca (loss of substituting cations), and an increase in the ratio  $\text{CaO}/\text{P}_2\text{O}_5$  (loss of the cations that replace Ca and replacement of  $\text{PO}_4^{3-}$  by  $\text{CO}_3^{2-}$ ).

*Weathering indices*

The spot analyses of unweathered samples of apatite reveal compositions similar to those established for fresh apatite, such as a  $\text{CaO}/\text{P}_2\text{O}_5$  value around 1.3, higher contents of cations substituting for Ca, and totals above 99 wt.%. Grain compositions from partially weathered samples are divided in two groups: one similar to the fresh apatite with totals above 99 wt.%, and the other similar to the supergene apatite, with totals below 98 wt.%. The same trends were found in a detailed study of individual grains showing signs of weathering, and were interpreted as indicative of incongruent dissolution of apatite, *i.e.*, some parts of the grains have had their composition affected by weathering, and are no longer identical to fresh apatite.

The values of the parameters mentioned above, which indicate the evolution among the different types of apatite and within the same type (primary apatite) at several stages of weathering, may be used as indices of weathering.

*Practical consequences*

The igneous origin and the influence of lateritization are two major differences between the phosphate ore in Brazil and that commonly exploited all over the world. Furthermore, lateritization is associated with the formation of apatite and non-apatite supergene phosphates and with profound changes in the morphology and texture of grains. The Brazilian carbonatitic complexes mineralized in apatite, such as Catalão I, present, in their lateritic mantle, several distinct types or generations of apatite, along with other newly formed phosphates, resulting in very heterogeneous ores. These features, typical of the lateritic environment, modify the density, the mechanical and physicochemical behavior of the apatite grains, as well as solubility, all of these factors with consequences in the industrial processes of apatite concentration (Barros 1997, Toledo *et al.* 1999, Ferrari *et*

al. 2001). Thus, lateritization acts by concentrating the apatite in the first stages of weathering, and, on the other hand, by promoting chemical and morphological changes that render difficult its industrial recovery.

Potentially toxic elements, such as U, Th and Cd, were not detected in the analytical data bearing on the various generations of apatite from Catalão I, nor in other Brazilian complexes described in the above-mentioned literature. This fact may be an important attribute of the predominantly igneous Brazilian phosphate ore in relation to some of the sedimentary ore exploited in the world and used in Brazil to fulfill the current needs of its phosphate industry.

#### ACKNOWLEDGEMENTS

The authors are grateful to J.P. Fortuné for making possible a post-doctoral stage at Université Paul Sabatier (Toulouse, France) for the first author, where an important part of data were obtained, and to Fosfértil Co. (Brazil) and C.C. Ribeiro, for authorization and help concerning the field work. This research was financially supported by FAPESP (95/6685-5 and 96/7868-9), CNPq (303796/86.3), and CAPES-COFECUB (169/95 and 309/00/02-II). The authors are also grateful to the anonymous referees for their helpful comments.

#### REFERENCES

- ALCOVER NETO, A. & TOLEDO, M.C.M. de (1993): Evolução supérgena do carbonatito de Juquiá (SP). *Revista do Instituto Geológico* **14**(1), 31-43.
- ALTSCHULER, Z.S. (1973): The weathering of phosphate deposits – geochemical and environmental aspects. In *Environmental Phosphorus Handbook* (E.J. Griffith, A. Beeton, J.M. Spencer & D.T. Mitchell, eds.). John Wiley & Sons, New York, N.Y. (33-96).
- AMARAL, G., BUSHEE, J., CORDANI, U.G., KAWASHITA, K. & REYNOLDS, J.H. (1967) Potassium-argon ages of alkaline rocks from southern Brazil. *Geochim. Cosmochim. Acta* **31**, 117-142.
- ARAÚJO, D.P. de & GASPAS, J.C. (1992): Química mineral dos carbonatitos e rochas associadas de Catalão I, GO. In *Anais 37<sup>th</sup> Congresso Brasileiro de Geologia*, São Paulo, Brazil (90-91).
- BARROS, L.A.F. de (1997): *Flotação da apatita da jazida de Tapira (MG, Brazil)*. M.Sc. thesis, Univ. de São Paulo, São Paulo, Brazil.
- BENY, C., BOULINGUI, B. & PIANTONE, P. (1996): Application de la spectrométrie Raman à la caractérisation des apatites du gisement de Mabounié, Gabon. *Terra Nova (suppl.)*, **8**, C1 (abstr.).
- BOULINGUI, B. (1997): *Minéralogie et géochimie du gisement résiduel de phosphore et niobium de Mabounié (Gabon)*. Ph.D. thesis, Institut National Polytechnique de Lorraine, Lorraine, France.
- BREWER, R. (1964): *Fabric and Mineral Analysis of Soils*. J. Wiley & Sons, New York, N.Y.
- CARVALHO, W.T. (1974): Aspectos geológicos e petrográficos do Complexo ultramáfico-alcalino de Catalão I, GO. *Anais 28<sup>th</sup> Congresso Brasileiro de Geologia (Porto Alegre)* **5**, 107-123.
- COMODI, P. & LIU, YU (2000): CO<sub>3</sub> substitution in apatite: further insight from new crystal-chemical data of Kasekere (Uganda) apatite. *Eur. J. Mineral.* **12**, 965-974.
- COSTA, C.N. DA, JR. (2002): *Dissolução química e biogeoquímica de apatita magmática*. Ph.D. thesis, Univ. de Brasília, Brasília, Brazil.
- DELMAS, A.-B. (1979): Apport de la cinétique dans la connaissance des phénomènes d'altération. *Bull. Assoc. Fr. Etude du Sol* **2-3**, 125-134.
- DELVIGNE, J.E. (1998): Atlas of Micromorphology of Mineral Alteration and Weathering. *Can. Mineral., Spec. Publ.* **3**.
- EBY, G.N. & MARIANO, A.N. (1986): Geology and geochronology of carbonatites peripheral to the Paraná Basin, Brazil-Paraguay. *Geol. Assoc. Can. – Mineral. Assoc. Can. – Can. Geophys. Union, Program Abstr.* **11**, 66.
- FERRARI, V.C. (2000): *Fosfatos primários e secundários nos perfis de intemperismo sobre os maciços de Juquiá, Anitópolis e Tapira*. Ph.D. thesis, Univ. de São Paulo, São Paulo, Brazil.
- \_\_\_\_\_, TOLEDO, M.C.M. de, SANTOS, C.N. dos & KAHN, H. (2001): Aspectos cristalóquímicos, mineralógicos e tecnológicos da apatita de Tapira (MG). *Geochimica Brasiliensis* **15**(1-2), 93-112.
- FLEET, M.E. & PAN, YUANMING (1995): Crystal chemistry of rare-earth elements in fluorapatite and some calc-silicates. *Eur. J. Mineral.* **7**, 591-605.
- FLICOTEAUX, R. & LUCAS, J. (1984): Weathering of phosphate minerals. In *Phosphate Minerals* (J.B. Nriagu & P.B. Moore, eds.). Springer-Verlag, Berlin, Germany (292-317).
- FRANSOLET, A.-M. & SCHREYER, W. (1981): Unusual, iron-bearing apatite from a garnetiferous pegmatoid, Northampton Block, Western Australia. *Neues Jahrb. Mineral., Monatsh.*, 317-327.
- HUGHES J.M., CAMERON M. & MARIANO A.N. (1991): Rare-earth-element ordering and structural variations in natural rare-earth-bearing apatites. *Am. Mineral.* **76**, 1165-1173.
- KOHN, M.J., RAKOVAN, J. & HUGHES, J.M., eds. (2002): Phosphates: Geochemical, Geobiological and Materials Importance. *Rev. Mineral. Geochem.* **48**.

- LAPIDO-LOUREIRO, F.E. DE V. (1995): *A mega província carbonatítica Brasil-Angola e seus recursos minerais – Geologia, Petrografia, Geoquímica, Geologia Econômica*. Ph.D. thesis, Univ. de Lisboa, Lisbon, Portugal.
- LARSEN, E.S., JR., FLETCHER, M.H. & CISNEY, E.A. (1952): Strontium apatite. *Am. Mineral.* **37**, 656-658.
- LE BAS, M.J. & HANDLEY, C.D. (1979): Variation in apatite composition in ijolitic and carbonatitic igneous rocks. *Nature* **279**, 54-56.
- LEHR, J.R., MCCLELLAN, G.H., SMITH, J.P. & FRAZIER, A.W. (1968): Characterization of apatites in commercial phosphate rocks. In *Colloque International sur les phosphates minéraux solides* (1967, Toulouse). *Bull. Soc. Chim. Fr., num. spécial*, 29-44.
- LENHARO, S.L.R. (1994): *Caracterização mineralógica/tecnológica das apatitas de alguns depósitos brasileiros de fosfato*. M.Sc. thesis, Univ. de São Paulo, São Paulo, Brazil.
- LEROY, G. (1997): Microcaractérisation de la phase minérale osseuse. *Innov. Tech. Biol. Med.* **18**, 151-165.
- LIU, YU & COMODI, P. (1993): Some aspects of the crystal-chemistry of apatites. *Mineral. Mag.* **57**, 709-719.
- MARSHALL, D.J., ed. (1988): *Cathodoluminescence of Geological Materials*. Unwin Hyman, Boston, Massachusetts.
- MCARTHUR, J.M. (1990): Fluorine-deficient apatite. *Mineral. Mag.* **54**, 508-510.
- MCCLELLAN, G.H. (1980): Mineralogy of carbonate fluorapatites. *J. Geol. Soc.* **137**, 675-681.
- \_\_\_\_\_, & LEHR, J.R. (1969): Crystal chemical investigation of natural apatites. *Am. Mineral.* **54**, 1374-1391.
- MITCHELL, R.H., XIONG, JIAN, MARIANO, A.N. & FLEET, M.E. (1997): Rare-earth-element-activated cathodoluminescence in apatite. *Can. Mineral.* **35**, 979-998.
- MUL, F.F., HOTTENHUIS, M.H., BOUTER, P., GREVE, J., ARENDS, J. & BOSCH, J.J. (1986): Micro-Raman line broadening in synthetic carbonated hydroxyapatite. *J. Dental Res.* **65**, 437-440.
- \_\_\_\_\_, OTTO, C., GREVE, J., ARENDS, J. & BOSCH, J.J. (1988): Calculation of the Raman line broadening on carbonatation in synthetic hydroxyapatite. *J. Raman Spectrosc.* **19**, 13-21.
- NELSON, D.G.A. & WILLIAMSON, B.E. (1982): Low-temperature laser Raman spectroscopy of synthetic carbonated apatites and dental enamel. *Aust. J. Chem.* **35**, 715-727.
- OLIVEIRA, S.M.B. de & IMBERNON, R.A.L. (1998): Weathering alteration and related REE concentration in the Catalão I carbonatite complex, central Brazil. *J. S. Am. Earth Sci.* **11**, 379-388.
- PENEL, G., LEROY, G., REY, C. & BRES, E. (1998): MicroRaman spectral study of carbonated apatites, enamel, dentine and bone. *Calcif. Tissue Int.* **63**, 475-481.
- PEREIRA, V.P. (1995): *Alteração no Maciço Alcalino-carbonatítico de Catalão I (GO, Brasil). Evolução mineralógica*. Ph.D. thesis, Univ. Federal do Rio Grande do Sul, Porto Alegre, Brazil.
- \_\_\_\_\_, FORMOSO, M.L.L. & TOLEDO, M.C.M. de (1997): Aspectos da alteração hidrotermal e intempérica no maciço alcalino-carbonatítico de Anitápolis. *Geochimica Brasiliensis* **11**, 187-205.
- PRINS, P. (1973): Apatite from African carbonatites. *Lithos* **6**, 133-144.
- RAE, D.A., COULSON, I.M. & CHAMBERS, A.D. (1996): Metasomatism in the north Qôroq centre, South Greenland: apatite chemistry and rare-earth element transport. *Mineral. Mag.* **60**, 207-220.
- REGNIER, P., LASAGA, A.C., BERNER, R.A., HAN, O.H. & ZILM, K.W. (1994): Mechanism of CO<sub>3</sub><sup>2-</sup> substitution in carbonate fluorapatite: evidence from FTIR spectroscopy, <sup>13</sup>C NMR and quantum mechanical calculations. *Am. Mineral.* **79**, 809-818.
- RIBEIRO, C.C. (1998): *Maciço de Catalão I, GO*. Unpubl. Rep., Ultrafértil, Brazil.
- RODRIGUES, C.S. & LIMA, P.R.A.S.L. (1984): Carbonatitic complexes of Brazil. In *Carbonatitic Complexes of Brazil: Geology*. Companhia Brasileira de Metalurgia e Mineração, São Paulo, Brazil (3-17).
- ROEDER, P.L., MACARTHUR, D., MA, XIN-PEI, PALMER, G.R. & MARIANO, A.N. (1987): Cathodoluminescence and microprobe study of rare-earth elements in apatite. *Am. Mineral.* **72**, 801-811.
- RØNSBO, J.G. (1989): Coupled substitutions involving REEs and Na and Si in apatites in alkaline rocks from the Ilímaussaq intrusion, South Greenland, and the petrological implications. *Am. Mineral.* **74**, 896-901.
- SCHIEB, R.M., THRASHER, R.D. & LEHR, J.R. (1984): Chemical composition determination of francolite apatites by Fourier Transform infrared (FTIR) spectroscopy. SPIE, 1981, 289-291.
- SCHWAB, R.G., HEROLD, H., COSTA, M.L. & OLIVEIRA, N.P. (1989): The formation of aluminous phosphates through lateritic weathering of rocks. In *Weathering: its Products and Deposits 2* (K.S. Balasubramanian & V.P. Evangelov, eds.). Theophrastus, Athens, Greece (369-386).
- SOMMERAUER, J. & KATZ-LEHNERT, K. (1985): A new partial substitution mechanism of CO<sub>3</sub><sup>2-</sup>/CO<sub>3</sub>OH<sup>3-</sup> and SiO<sub>4</sub><sup>4-</sup> for the PO<sub>4</sub><sup>3-</sup> group in hydroxyapatite from the Kaiserstuhl alkaline complex (SW-Germany). *Contrib. Mineral. Petrol.* **91**, 360-368.

- SONOKI, I.K. & GARDA, G.M. (1988): Idades K–Ar de rochas alcalinas do Brasil Meridional e Paraguai Oriental. Compilação e adaptação às novas constantes de decaimento. *Boletim Instituto de Geociências Univ. São Paulo* **19**, 63-85.
- TOLEDO, M.C.M. de (1999): *Mineralogia dos principais fosfatos do Maciço Alcalino-carbonatítico de Catalão I (GO) e sua evolução no perfil laterítico*. Livre Docência Thesis, Univ. de São Paulo, São Paulo, Brazil.
- \_\_\_\_\_ (2000): O grupo da crandallita no manto laterítico sobre o maciço carbonatítico de Catalão I (GO, Brasil). *Geochimica Brasiliensis* **14**, 71-95.
- \_\_\_\_\_, DE PARSEVAL, P., FONTAN, F., LEROY, G. & RIBEIRO, C.C. (1998): Caractérisation des apatites de différentes générations du massif alcalin-carbonatitique de Catalão I (Goiás, Brasil). *Bol. Soc. Esp. Mineral.* **21**–A, 202-203.
- \_\_\_\_\_, FERRARI, V.C., ALCOVER NETO, A., FONTAN, F., MARTIN, F., SANTOS, C.N. DOS & CARVALHO, F.M.S. (2002): Fosfatos aluminosos com ferro do grupo da crandallita nas coberturas lateríticas de Catalão I, Juquiá e Tapira, Brasil, e Chiriguélo, Paraguai. *Revista Brasileira de Geociências* **32**, 389-402.
- \_\_\_\_\_, \_\_\_\_\_, SANTOS, C.N. DOS & ALCOVER NETO, A. (1997): Aspectos geoquímicos da gênese dos fosfatos secundários associados ao Maciço Alcalino-carbonatítico de Juquiá (SP). In Abstr. Vol., 5<sup>th</sup> Congresso Brasileiro de Geoquímica (Salvador).
- \_\_\_\_\_, \_\_\_\_\_, \_\_\_\_\_, \_\_\_\_\_, DE PARSEVAL, P., FONTAN, F. & RIBEIRO, C.C. (1999): Lateritic weathering effects over phosphatic Brazilian ores: Catalão I and Juquiá (Brasil). In Abstr. Vol., 19<sup>th</sup> Int. Geochem. Explor. Symp. (Vancouver), 142-143.
- \_\_\_\_\_ & PEREIRA, V.P. (2001): A variabilidade de composição da apatita. *Rev. Instituto Geológico* **22**(1–2), 27-64.
- TRELOAR, P.J. & COLLEY, H. (1996): Variations in F and Cl contents in apatites from magnetite–apatite ores in northern Chile, and their ore-genetic implications. *Mineral. Mag.* **60**, 285-301.
- TSUDA, H. & ARENDS, J. (1994): Orientational micro-Raman spectroscopy on hydroxyapatite single crystals and human enamel crystallites. *J. Dent. Res.* **73**, 1703-1710.
- VIEILLARD, P., TARDY, Y. & NAHON, D. (1979): Stability fields and aluminum phosphates: parageneses in lateritic weathering of argillaceous phosphatic sediments. *Am. Mineral.* **64**, 626-634.
- VIGNOLES, M. & BONEL, G. (1978): Sur la localisation des ions fluorure dans les carbonate-apatites de type B. *C.R. Acad. Sci. Paris* **287**, sér. C, 321-324.
- YOUNG, E.J., MYERS, A.T., MUNSON, W.L. & CONKLIN, N.M. (1969): Mineralogy and geochemistry of fluorapatite from Cerro de Mercado, Durango, Mexico. *U.S. Geol. Surv., Prof. Pap.* **650-D**, 84-93.

Received November 7, 2003, revised manuscript accepted July 25, 2004.